

BLAST RETROFIT DESIGN OF CMU WALLS USING POLYMER SHEETS

---

A Thesis Presented to the Faculty of the Graduate School of the  
University of Missouri – Columbia

---

In Partial Fulfillment of the Requirements for the Degree

Master of Science

In

Civil and Environmental Engineering

---

By

SILAS JAMES FITZMAURICE

Dr. Hani Salim, Thesis Supervisor

May 2006

## ***ACKNOWLEDGEMENTS***

I would like to formally thank my adviser Dr. Hani Salim, Professor of Civil and Environmental Engineering at the University of Missouri-Columbia for his invaluable guidance and guidance throughout the entirety of this research. Dr. Salim has work countless hours including nights and weekends providing me with encouragement and insight into this project. He is truly a brilliant Professor of Civil Engineering and a good friend. Without Dr. Salim this research would not be possible.

I would also like to thank the United States Air Force Research Laboratory for providing the funding for this research. Also, the Air Force Lab provided coupon data and live testing data for this thesis. Additionally, I am grateful for the insight and effort Dr. Robert Dinan has contributed to this project.

I am also grateful to Dr. Sherif El-Gizawy, Dr. Glenn Washer, and Dr. Hani Salim for taking time out of their day to serve on my defense committee.

I would also like to thank my fellow students who help me build setups for my experimental testing. I would especially like to thank John Hoemann for spending his time helping conduct experiments on weekends and adding his insight whenever possible. Additionally, Matt Oesch, Rhett Johnson, Chance Baragary, Tyler Oesch and all who have helped me with immensely with the amount of work that was done for this research.

Finally, and most importantly, I would like to thank God, my family, and friends for their support throughout my education.

## TABLE OF CONTENTS

<b>ACKNOWLEDGEMENTS</b> .....	ii
<b>LIST OF FIGURES</b> .....	vi
<b>LIST OF TABLES</b> .....	x
<b>ABSTRACT</b> .....	xi
<b>Chapter 1 Introduction</b> .....	1
1.1 General.....	1
1.2 Purpose and Scope .....	2
1.3 Approach.....	3
<b>Chapter 2 Review of Literature</b> .....	4
2.1 General.....	4
2.2 Technical Background .....	4
2.3 Previous Blast Resistant Research.....	6
<b>Chapter 3 Analytical Modeling of the Static Resistance Function of Polymer sheets</b> .....	11
<b>Chapter 4 Experimental Evaluation</b> .....	21
4.1 General.....	21
4.2 Coupon Testing.....	21
4.2.1 Setup and Procedure .....	21
4.2.2 Calculating True Stress from Engineering Stress.....	22
4.2.3 Results.....	23

4.2.4	Summary and Conclusions .....	25
4.3	Connection Testing .....	25
4.3.1	General .....	25
4.3.2	Setup and Procedure .....	26
4.3.3	Results .....	29
4.3.4	Summary and Conclusions .....	45
4.4	Component Beam Testing .....	47
4.4.1	General .....	47
4.4.2	Setup and Procedure .....	47
4.4.3	Results .....	51
4.4.4	Summary and Conclusion .....	55
<b>Chapter 5</b>	<b>Dynamic Modeling .....</b>	<b>57</b>
5.1	General .....	57
5.2	SDOF Dynamic Modeling .....	58
5.3	Appication of the Dynamic Model .....	63
5.4	Field Testing .....	69
5.4.1	Polymer Sheets .....	70
5.4.1.1	Test Setup .....	70
5.4.1.2	Results .....	72
5.4.2	CUE Polymer .....	76
5.4.2.1	Test Setup .....	76
5.4.2.2	Prediction .....	79
5.4.2.3	Results .....	81

5.4.3 Bayer Polymer .....	82
5.4.3.1 Test Setup.....	82
5.4.3.2 Prediction .....	84
5.4.3.3 Results .....	86
5.5 Summary and Conclusion.....	87
Chapter 6 <b>Conclusions and Recommendations</b> .....	88
<b>References</b> .....	90

## LIST OF FIGURES

<b>Figure 2.1:</b> Typical Blast Loading .....	5
<b>Figure 2.2:</b> Small-scale testing of polymer retrofitted concrete beams. Weak bond allows polymer to stretch without tearing (top), whereas a strong bond causes polymer to tear at initial crack location in concrete (bottom). .....	9
<b>Figure 2.3:</b> Average normalized Load-Displacement curve of concrete samples. Graph is normalized with respect to peak response of Non-retrofitted samples ....	10
<b>Figure 3.1:</b> Free body diagram and deflected shape of sample .....	12
<b>Figure 3.2:</b> Flowchart for the derivation of pressure-deflection relationship .....	13
<b>Figure 3.3a:</b> True Stress (Left) vs. Engineering Stress (Right) .....	19
<b>Figure 3.4b:</b> Static Resistance Function of Polymer of Figure 3.3a.....	20
<b>Figure 4.1:</b> Coupon testing setup .....	21
<b>Figure 4.2:</b> True Stress (Left) vs. Engineering Stress (Right) for LS V1a .....	23
<b>Figure 4.3:</b> Stress-strain results of tensile tests on coupon samples .....	24
<b>Figure 4.4:</b> AutoCAD depiction of the connection test setup.....	26
<b>Figure 4.5:</b> Picture of the connection setup .....	27
<b>Figure 4.6:</b> Failure of Polymer Sample.....	28
<b>Figure 4.7:</b> Test sample LS-C1b.....	30
<b>Figure 4.8:</b> Load-deflection curve for LS-C1b .....	30
<b>Figure 4.9:</b> Test sample LS-C2.....	31
<b>Figure 4.10:</b> Load-deflection curve for LS-C2 .....	31
<b>Figure 4.11:</b> Test sample LS-C2b.....	32

<b>Figure 4.12:</b> Load-deflection curve for LS-C2b .....	32
<b>Figure 4.13:</b> Test sample LS-C3 .....	33
<b>Figure 4.14:</b> Load-deflection curve for LS-C3 .....	33
<b>Figure 4.15:</b> Test sample LS-C3b .....	34
<b>Figure 4.16:</b> Load-deflection curve for LS-C3b .....	34
<b>Figure 4.17:</b> Test sample LS-C4b .....	35
<b>Figure 4.18:</b> Load-deflection curve for LS-C4b .....	35
<b>Figure 4.19:</b> Test sample LS-C5 .....	36
<b>Figure 4.20:</b> Load-deflection curve for LS-C5 .....	36
<b>Figure 4.21:</b> Test sample LS-C5b .....	37
<b>Figure 4.22:</b> Load-deflection curve for LS-C5b .....	37
<b>Figure 4.23:</b> Test sample LS-C6 .....	38
<b>Figure 4.24:</b> Load-deflection curve for LS-C6 .....	38
<b>Figure 4.25:</b> Test sample LS-C6b .....	39
<b>Figure 4.26:</b> Load-deflection curve for LS-C6b .....	39
<b>Figure 4.27:</b> Test sample LS-C7b .....	40
<b>Figure 4.28:</b> Load-deflection curve for LS-C7b .....	40
<b>Figure 4.29:</b> Test sample LS-C8 .....	41
<b>Figure 4.30:</b> Load-deflection curve for LS-C8 .....	41
<b>Figure 4.31:</b> Test sample LS-C8b .....	42
<b>Figure 4.32:</b> Load-deflection curve for LS-C8b .....	42
<b>Figure 4.33:</b> Test sample LS-C9 .....	43
<b>Figure 4.34:</b> Load-deflection curve for LS-C9 .....	43

<b>Figure 4.35:</b> Test sample LS-C10.....	44
<b>Figure 4.36:</b> Load-deflection curve for LS-C10.....	44
<b>Figure 4.37a:</b> AutoCAD Drawling of the 16-Point Loading Tree.....	48
<b>Figure 4.37b:</b> Polymer Sample at the Beginning of the Test.....	49
<b>Figure 4.37c:</b> Polymer Sample Nearing the End of the Test .....	49
<b>Figure 4.37d:</b> Connection at the Beginning (Left) and During the Test (Right).....	50
<b>Figure 4.38:</b> Location of Displacement Devices for Component Beam Tests .....	51
<b>Figure 4.39:</b> Comparison of the Experimental vs. Analytical Data for LS-T1.....	52
<b>Figure 4.40:</b> Comparison of the Experimental vs. Analytical Data for LS-T2.....	53
<b>Figure 4.41:</b> Comparison of the Experimental vs. Analytical Data for LS-T3.....	54
<b>Figure 4.42:</b> Comparison of the Experimental vs. Analytical Data for LS-T4.....	55
<b>Figure 5.1:</b> Beam Idealized as SDOF Mass and Spring System .....	58
<b>Figure 5.2:</b> Free Body Diagram (FBD) of the Mass.....	59
<b>Figure 5.3:</b> Pressure-time plot of a blast event .....	60
<b>Figure 5.4:</b> Negative Loading Region Idealized.....	61
<b>Figure 5.5a:</b> Partial Calculation of the SDOF Model Using Excel .....	64
<b>Figure 5.5b:</b> The Opening screen of AFWAC.....	66
<b>Figure 5.6:</b> Resistance of a CMU Wall with and without Arching.....	67
<b>Figure 5.7:</b> Deflection vs. Time with Varying CMU Wall resistances.....	68
<b>Figure 5.8:</b> Effects of the Negative Phase on Wall Response .....	69
<b>Figure 5.9:</b> Schematic of the CMU Wall with Polymer Sheet Retrofit .....	70
<b>Figure 5.10:</b> CMU Wall with and without Polymer Sheet Retrofit.....	71
<b>Figure 5.11:</b> Outside and Inside of Wall after Explosion .....	72



<b>Figure 5.12a:</b> Analytical Model of the Static Resistance Function.....	73
<b>Figure 5.12b:</b> Stress-Strain Relationship for the LifeShield Polymer .....	73
<b>Figure 5.13:</b> Pressure and Impulse versus Time for Gage R2 .....	74
<b>Figure 5.14:</b> Pressure and Impulse versus Time for Gage R3 .....	75
<b>Figure 5.15:</b> Pressure and Impulse versus Time for Gage R4 .....	75
<b>Figure 5.16:</b> Comparison of the Predicted SDOF Model to the Actual response.....	76
<b>Figure 5.17:</b> CMU Wall with CUE Polymer Retrofit.....	77
<b>Figure 5.18:</b> CUE Polymer Connection.....	78
<b>Figure 5.19:</b> Outside of CMU Wall after Explosion.....	78
<b>Figure 5.20:</b> Coupon Testing of a CUE Sample .....	79
<b>Figure 5.21:</b> Coupon Results of a Typical CUE Sample .....	80
<b>Figure 5.22:</b> Analytical Model of the CUE Polymer Sheets.....	80
<b>Figure 5.23:</b> Loading Function from the Pressure Gage.....	81
<b>Figure 5.24:</b> Comparison of the Predicted SDOF Model to the Actual response.....	82
<b>Figure 5.25:</b> CMU Wall with Bayer Polymer Retrofit .....	83
<b>Figure 5.26:</b> CMU Wall Retrofitted with Bayer Polymer after Explosion.....	84
<b>Figure 5.27:</b> Typical Coupon Results of Bayer Polymer.....	85
<b>Figure 5.28:</b> Analytical Model of Bayer Retrofit System.....	85
<b>Figure 5.29:</b> Loading Function from the Pressure Gage.....	86
<b>Figure 5.30:</b> Comparison of the Predicted SDOF Model to the Actual response.....	87

## LIST OF TABLES

<b>Table 4.1:</b> Coupon test results for Life Shield (LS) samples .....	24
<b>Table 4.2:</b> Results from Connection Testing .....	29
<b>Table 4.3:</b> Theoretical Capacity Compared with Experimental Capacity .....	47
<b>Table 4.4:</b> Component Beam Test Matrix.....	48

# BLAST RETROFIT DESIGN OF CMU WALLS USING POLYMER SHEETS

Silas James Fitzmaurice

Dr. Hani Salim, Thesis Supervisor

## **ABSTRACT**

Many materials have been tested for blast retrofit design but have shown to have limitation. The focus of this research is the analysis of polymer sheets as a method for retrofit design. There are many advantages of polymer sheets, such as the sheets are very thin and take up very little space, polymer have large amount of energy absorption capabilities, and the installation process is quick and easy to perform in the field.

This research is done to ascertain the strength, ductility, response to static pressure, investigate connection details, and develop an analytical model of the static resistance function. The polymer retrofit system is modeled dynamically in a single-degree of freedom (SDOF) model. The analytical model developed for the static resistance is used in the SDOF model. Additionally, three types of test were conducted at the coupon, connection, and component levels to verify the analytical model. Once the analytical model is verified, it is incorporated into the SDOF model. Additionally, field testing was conducted on three polymers and results were compared to the predicted result made by this project. This thesis presents the analytical modeling and experimental evaluation of CMU-polymer walls to blast loading.

# CHAPTER 1 -- INTRODUCTION

## 1.1 General

Due to the increasing need for blast resistant structures, many retrofit systems have been developed to increase the energy absorption of typical infill concrete masonry unit (CMU) walls. CMU walls are chosen because they are commonly used in the field and easy to construct. Most CMU walls are designed for typical structural loads like dead loads, live loads, wind loads, and snow loads. Accordingly, they have very low resistances to blast loading and fail catastrophically under blast pressure producing hazardous projectiles that enter the room. Blast loading is unlike any other type of load; they are short in duration and high in pressure. One important property of a blast is the reflected impulse. Generally, the reflected impulse is what governs the design and not the peak pressure (Stone and Engebretsen, 2001). Because the reflected impulse is what governs and not the peak pressure, the retrofit material does not necessarily have to have high strength, but must be very ductile and have high energy absorption capabilities. Many steel retrofit systems have been investigated and proven to be effective, such as steel studs (Dinan, 2005) and steel sheathing (Kennedy, 2005). Also, many polymer retrofit systems have been evaluated and determined to be effective, such as spray-on and trowel-on polymers (Beckman, 2004 and Davidson, 2005) and fiber reinforced polymers (Albert, 2001). For this project, polymer sheets will be evaluated as means to enhance the ductility and energy absorption of an infill masonry wall system. Instead of spraying or troweling the polymer to the wall, the polymer will be installed using long sheets that span the full length of the wall and anchored to the top and bottom floors using mechanical connections. To advance this technology and material for blast-retrofit of

CMU walls, it is necessary to develop an engineering design methodology and response prediction models under blast loads. Therefore, the objective of this research is to develop an analytical model to be used in a single-degree of freedom model which predicts the midspan deflection of the CMU wall and polymer system under blast loads.

## **1.2 Purpose and Scope**

The purpose of this research is to develop the static resistance function of polymer sheets under uniform pressure. In order to develop the static resistance function, many tasks must be performed. The first task is to analytically predict the response of the polymer sheets to uniform pressure. The second task, is to perform experimental tests at three levels. The first test series is at the coupon level, which is needed in order to find the stress-strain relationship of the polymer sheets. Next, connection test series will be performed to ensure that the polymer sheets will not fail at the connection which would inhibit the polymer to develop its full capacity. Finally, component tests will be conducted in order to experimentally verify the analytical resistance function developed. The third task, a dynamic model will be developed using the experimental and analytical data to determine the suitability of the polymer to resist blast loading. The fourth task, the model will be compared to field data collected from tests performed by The United States Air Force Research Lab (AFRL) at Tyndall Air Force Base FL. Finally, the results will be implemented into the PC-Code AFWAC to be used for future engineering design.

### **1.3 Approach**

In an effort to predict the behavior of the polymer sheets, an analytical model will be developed. The analytical model, or static resistance function, will predict the pressure-deflection graph for the polymer sheets. The analytical model will then be compared to the experimental data, obtained by using a 16-point loading tree simulating a uniform pressure loading.

Coupon tests on samples cut from polymer sheets were tested under uniaxial tension to failure using a constant head speed of 2 inches per minute. ASTM D638 standard was used to prepare and test the samples. The testing parameters for the connection tests are the two gage thicknesses of the polymer sheets, bolt spacing, and connection plate thicknesses. From the connection tests, an optimal combination of the parameters will be found and used for the component tests. For the component tests, two gage thicknesses of the polymer sheet, the optimal connection plate thickness, and the optimal bolt spacing will be used. Load-deflection response of the component tests will be recorded and used to verify the analytical model developed. The load-deflection curves developed in these component tests will be used to calculate the equivalent pressure-displacement response (Static Resistance Function) of the blast mitigation system, which is useful for predicting the dynamic response of the blast-retrofitted wall system.

# CHAPTER 2 – LITERATURE REVIEW

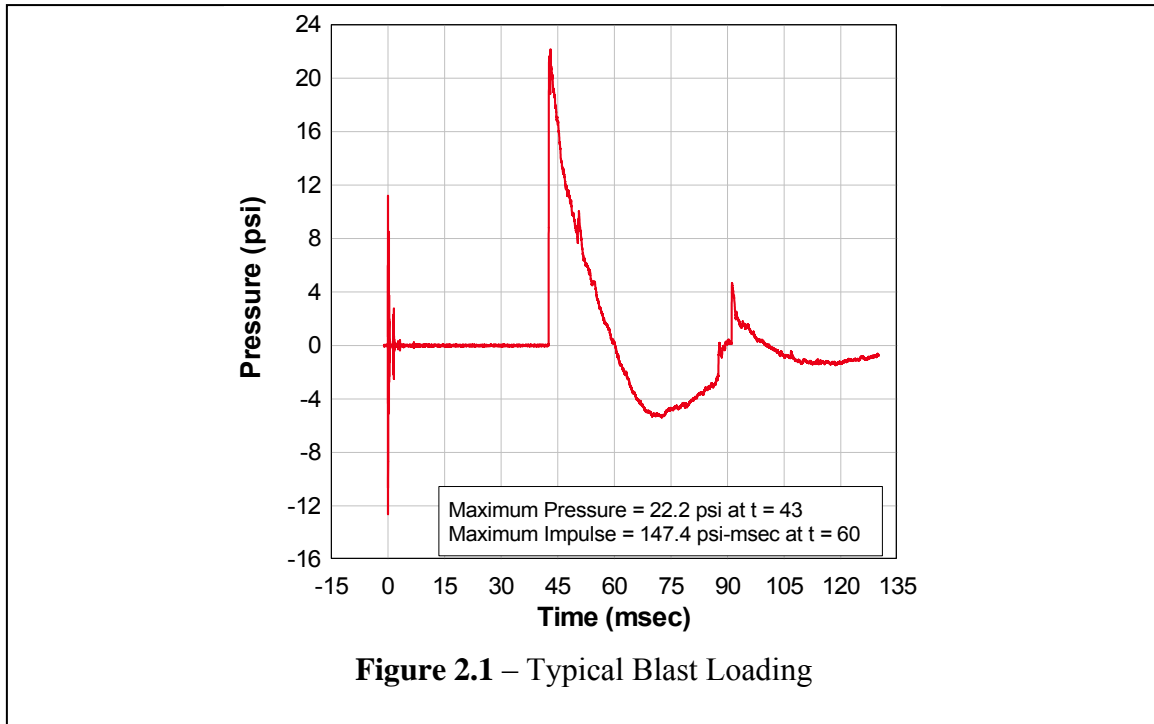
## 2.1 General

Due to an increase in the number of bombing threats, significant research has been conducted in an effort to retrofit structures to resist blast loading. The idea behind the retrofit systems is that they are inexpensive, easy to install, and they protect the occupants of the facilities. Several retrofit systems that have already been explored are the use of steel studs, steel sheets, fiber reinforced polymers, and trowel-on and spray-on polymers. Many papers and publications have been written on each of these retrofit systems.

## 2.2 Technical Background

To evaluate a blast retrofit design, it is crucial to understand the mechanics of a blast load and how a structure will react to the load. A blast loading comes from an explosion, which is defined as a rapid release of energy in the form of light, heat, sound, and a shockwave (Stone and Engebretsen, 2001). This shock wave released from the blast expands radially out from the source causing extremely large loading on the target structure. These targets, which are generally buildings, are typically only designed for wind load, which can cause pressures ranging in magnitude from 0.3 to 0.5 psi. However, blast loading can cause pressure typically ranging in magnitude from 30 to 50 psi, depending on size of bomb, distance from target, and angle of incidence. A typical blast event is shown in Figure 2.1. From the figure, it can be seen that there is a positive and a negative phase. The positive phase of the blast loading has duration of 15

milliseconds. The negative phase which typically reduces damage caused by the blast is typically ignored, in this thesis the effects of this region will be evaluated.



Although blast loads have extremely high peak pressure, the duration of these pressures are very short, which is advantageous in the design. Typically structures are designed for peak loading, but for blast-resistant structures, the duration is so short compared to the natural period that the blast impacts the structure and is gone before the structure responds significantly. This means the structure feels no peak pressure but feels the energy imparted by the blast. The reason for this is the natural period of a concrete structure is typically in the range of 100 to 200 milliseconds and a blast only last 15 milliseconds. Instead of designing the structure for peak pressures, it is designed to withstand the energy of the blast. Additionally, typical structures are designed using the assumption that the members are linearly elastic whether there in the elastic or plastic



range. This keeps deflection limits low causing low energy-absorption. For blast design, methodologies must allow the structure to undergo permanent plastic deformations to increase the energy absorption capabilities (Dinan, 2005).

### **2.3 Previous Blast Retrofit Research**

Much research has been done retrofitting systems for blast loading. Specifically, retrofit of non-load bearing concrete masonry units (CMU) walls have been the main focus of such research. The reason for this focus is that these walls are frequently used in construction and when introduced to blast loading they tend to cause a great deal of fragmentation under low pressures (Davidson et al., 2005). Below is an overview of the work done for the design of blast-retrofitted structures.

One of these retrofit systems investigated was the use of steel sheeting for blast retrofit design done by Kennedy (2005). In this research, thin steel sheets of various parameters were tested and performance was evaluated for blast design. The parameters included gages of steel sheathing, bolt spacing of connection, welded or bolted connection, and thickness of the connection plate. A static resistance function was developed and implemented into a dynamic modeling system. The modeling system would then, given blast loading parameters, predict the behavior of the wall retrofit system. The research provided conclusive evidence that the steel sheathing system could adequately resist blast loading (Kennedy, 2005).

Additionally, extensive research has been conducted in using polymers for blast retrofit design. In December 2000, a team of researchers tested three full-scale tests to determine the effectiveness of polymers to improve the blast resistance of unreinforced masonry walls. Some of the walls were reinforced with polymers and some were not and

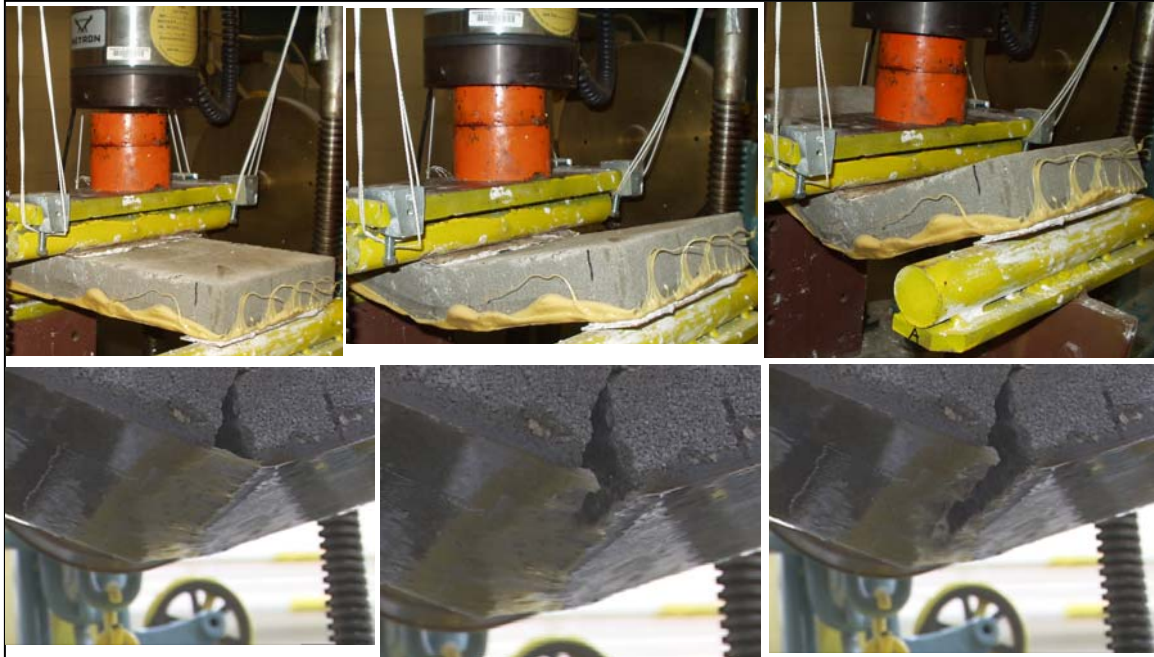
used as control walls to test the effectiveness of the polymers. The tests were designed to (1) evaluate the elastomeric polymer application process; (2) measure deflections at critical wall locations; (3) measure internal and external pressures created by the blast; (4) determine the failure modes; (5) assess the general effectiveness and level of protection provided by the elastomeric polymer retrofit (Davidson et al., 2004). The polymers used in these tests were spray-on polymers chosen based on stiffness, ductility, fire resistance, and cost. Three explosive tests were conducted on the polymers. In each of the tests an explosive charge was placed a certain distance away from the reinforced and unreinforced structures. These parameters were not released by the research team due to the sensitive nature of the project. The tests conclude that sprayed-on polymer retrofit approach for strengthening masonry wall systems against blast loads can be effective. However, these materials were deemed a poor choice due to high cost, difficulty adhering the material to the wall, and anchoring the material to the surrounding structure (Davidson et al., 2004).

Another paper by Davison (2005) discussed the damage and failure mechanisms observed from twelve polymer-reinforced masonry walls. The tests were to establish the limits of blast resistance effectiveness of polymer-reinforced masonry walls. The main observations of Davidson (2005) indicate that: (1) Thin elastomeric coating on the interior wall can eliminate secondary fragmentation and aid in preventing a collapse of the masonry wall. (2) A spray overlap of 6 inches of the polymer onto the surrounding structure provides enough strength to transfer loads from a blast to the structural frame to prevent collapse of polymer-reinforced masonry wall. (3) Although an effective balance should be maintained between stiffness and elongation ability, the elongation capacity is

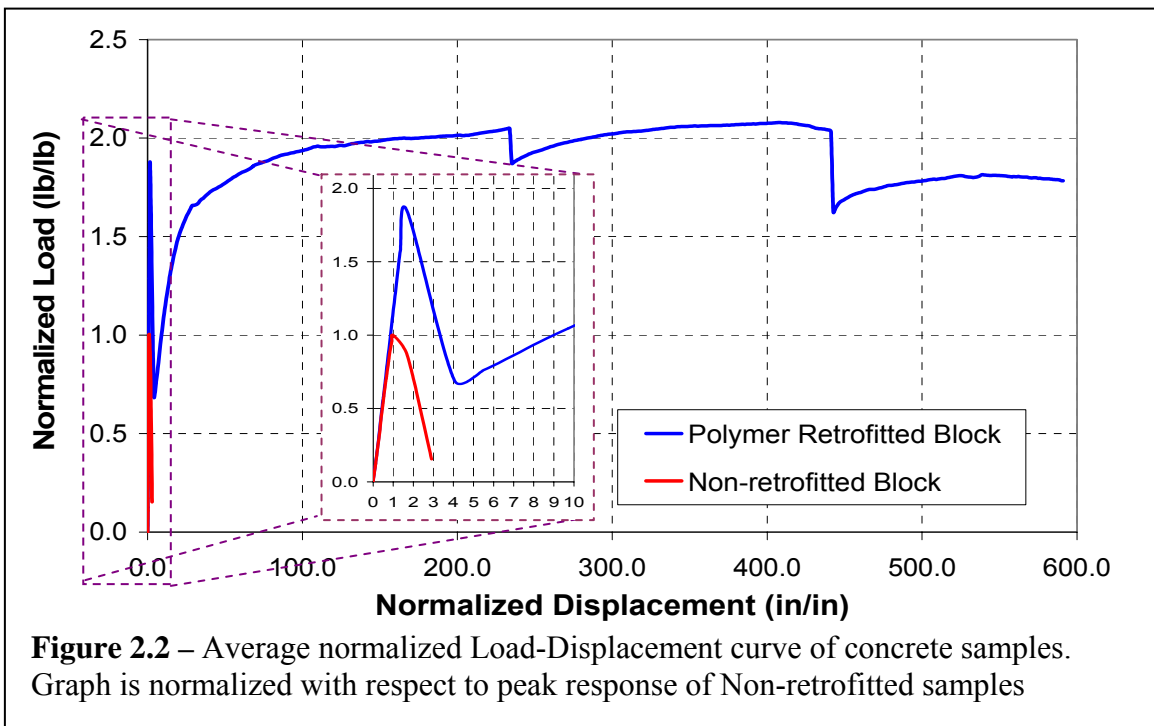
more important for this purpose than having a high stiffness. Additionally, a better balance between stiffness, shear tearing resistance, strength, and strain capacity should result in a more effective reinforcement. (4) Spray on polymer used in the test bonded well to the masonry. However this could cause concentrated stains at mortar joints and minimal strains to most of the polymer. An optimized balance between bond strength, strain energy absorption, and overlap strength may result in a more effective reinforcement system. Similar results were reported by Beckman (2005). (5) Front face shell fracture of the masonry of polymer-reinforced walls is common when the peak load is close to the loading capacity of the polymer-reinforced wall. This behavior should be further tested when considering the development of the static resistance function. (6) Significant arching effects were evident in some of the tests. Finite element results indicate that tight fit of the wall and the host frame is needed for significant arching stiffness to occur. Mortar in the joints provides freedom of movement that reduces arching effects. (7) A strong bond between the polymer and the wall was crucial in the effectiveness of the wall system. Without this the material resulted in tearing at the connection of the polymer coating to the host structure and collapse of the wall. However, a catcher membrane approach offers the potential advantage of more-efficiently absorbing strain energy over the greater reinforcement volume, as well as the use of a wide range of more cost effective material (Beckman 2005 and Bechtold 2004). (8) Both finite element results and posttest analyses indicate that the upper-most mortar joints fracture in the early stages of flexure, resulting in relative displacement of the two courses of block causing high shear strains in the polymer. This shows the importance of shear tearing resistance in an external reinforcement product. (9) For the masonry

structures considered in this study , the rate of strain in the polymer was significant, but not high. Finite element indicates a maximum strain rate is below  $100 \text{ s}^{-1}$ . (10) For walls with window or door openings, some effects were noted. A larger area of front face shell fracture, a tendency for tearing to initiate at the door or window frame, and additional breaching was observed. However, the overall effectiveness of the polymer remained high. Although the effectiveness of the polymer is very high, it should still be noted that there are still several problems. The polymers when sprayed emit toxic volatiles and requires protective clothing. Additionally, the equipment use is expensive and can be difficult to operate (Davidson et al., 2005).

Based on the research conducted by Beckman (2005) and Bechtold (2004) on small-scale concrete beams retrofitted with polymer sheets, the blast resistance is mostly attributed to the increased energy-absorption capability of the polymer (Figures 2.1 and 2.2). The research also indicates that a weak bond or no bond between the polymer and concrete wall is needed to obtain desirable performance. Strong bond between the polymer and the wall could cause the polymer to tear prematurely due to large localized elongation at the location of the crack (Beckman, 2005). No bond can be achieved easily in the case of polymer sheets, whereas weak bond can be achieved by painting the wall prior to spraying or toweling the polymer on the CMU wall.



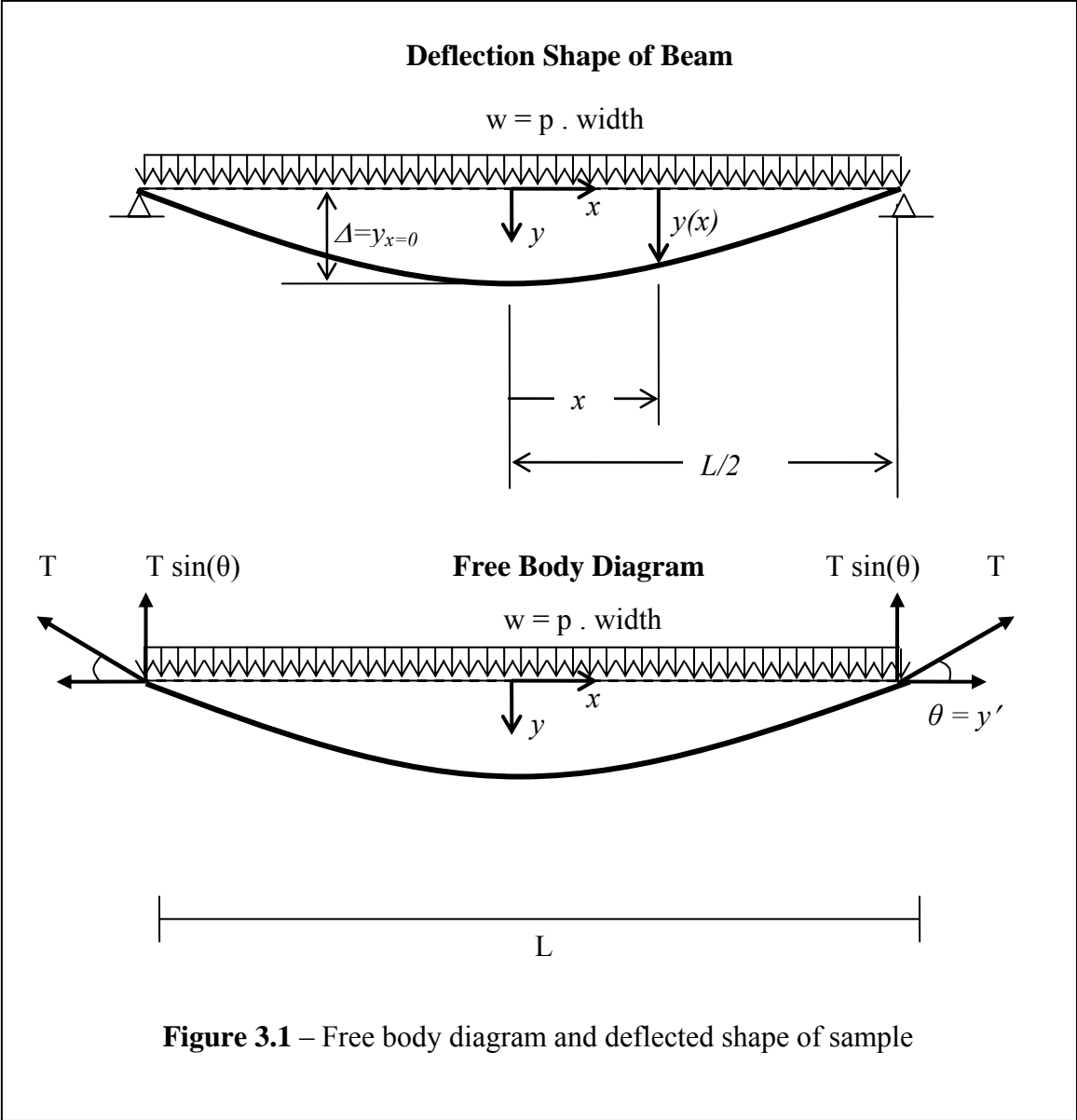
**Figure 2.1** – Small-scale testing of polymer retrofitted concrete beams. Weak bond allows polymer to stretch without tearing (top), whereas a strong bond causes polymer to tear at initial crack location in concrete (bottom)



**Figure 2.2** – Average normalized Load-Displacement curve of concrete samples. Graph is normalized with respect to peak response of Non-retrofitted samples

# **CHAPTER 3 – ANALYTICAL MODELING OF THE STATIC RESISTANCE FUNCTION OF POLYMER SHEETS**

To derive the exact analytical model, four principle steps will be followed to find pressure in terms of deflection. The first step is to assume a deformed shape of the polymer sheets under uniform loading (Figure 3.1). The deflected shape is assumed to be parabolic in nature (Lane, 2003). Once the deformed shape has been established, a free body diagram will be made and equilibrium will be used to find a relationship between load and stress. Next, using the coupon data and the constitutive relation between stress and strain, a relationship will be found between pressure and stress. Finally, a compatibility relationship between deflection and strain is analyzed, ultimately resulting in the desired relationship between pressure and deflection, the static resistance function. This process is outlined through the flow chart in Figure 3.2.



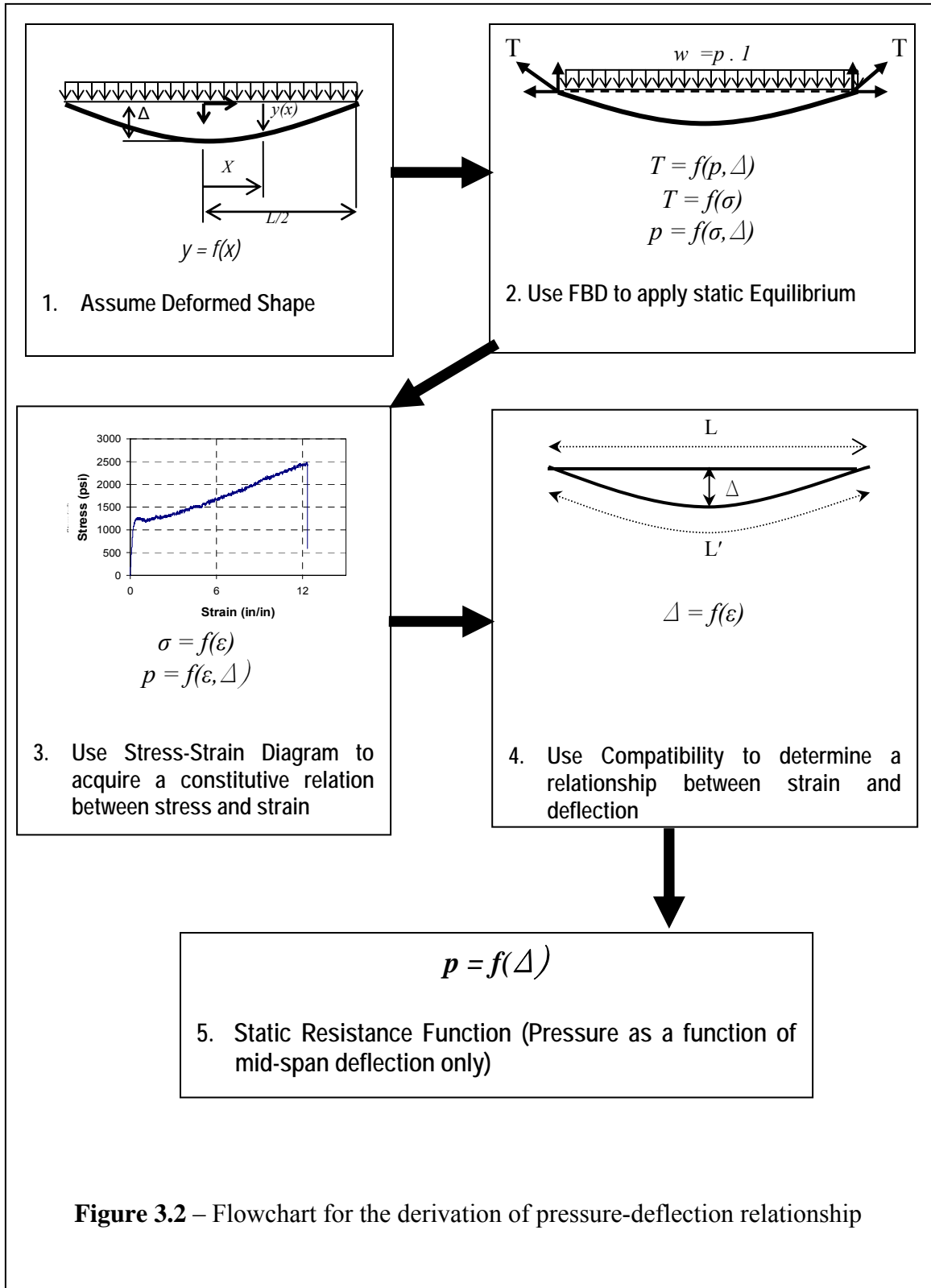


**Figure 3.2** – Flowchart for the derivation of pressure-deflection relationship



Since the assumed shape is parabolic, the derivation will begin with the general expression for a parabolic function to represent deflection as a function of x:

$$y = ax^2 + bx + c \quad (3.1)$$

Using known boundary conditions, constants a, b, and c will be determined. First b will be determined; to do this the derivative of equation 3.1 will be found.

$$y' = 2ax + b = 0,$$

The first boundary condition is

$$y' = 0 @ x = 0,$$

which results in

$$b = 0.$$

Now equation 3.1 reduces to,

$$y' = ax^2 + c$$

The second boundary condition is

$$y = \Delta @ x = 0$$

Substituting gives,

$$y = \Delta = a(0)^2 + c$$

or  $c = \Delta$

The final boundary condition is,

$$y = 0 @ x = \frac{L}{2}$$

Substituting gives,

$$y = a \left( \frac{L}{2} \right)^2 + \Delta = 0,$$

$$\text{or } a = -\frac{4\Delta}{L^2}.$$

Substituting constants a, b, and c back into equation 3.1 gives the expression for y and y' as shown below:

$$y(x) = \Delta \left( 1 - 4 \left( \frac{x}{L} \right)^2 \right) \quad (3.2)$$

$$y'(x) = 8\Delta \left( \frac{x}{L} \right) \quad (3.3)$$

Now that the parabolic shape is found, the next step is to use equilibrium to find a relationship between load and stress. From earlier research (Kennedy, 2005 and Dinan, 2005), it was found that the tension membrane force T varies along the length of the member with the smallest values at the mid point and the largest at the supports, which can vary up to approximately 10%. For simplicity, the tension force T will be assumed to be constant and the end values will be used (Kennedy, 2005).

In Figure 3.1 the free body diagram of the polymer sheets can be seen. From equilibrium it is known that,

$$\begin{aligned} \Sigma F_y &= 0 \\ \text{or } 2 T \sin(\theta) &= wL \end{aligned} \quad (3.4)$$

and for small angles,  $\sin(\theta)$  can be approximated as  $\theta$ , which is also equal to  $y'$  from equation 3.3. Additionally, T can be rewritten as  $\sigma A$ . Substituting this into equation 3.4 yields,

$$2(\sigma A) \left( \frac{-8\Delta}{L^2} x \right) = wL$$

Substituting  $x = \frac{L}{2}$ ,

$$2(\sigma A) \left( \frac{-8\Delta}{L^2} \frac{L}{2} \right) = wL$$

which simplifies and reduces to

$$\left( \frac{8\sigma A}{L^2} \right) \Delta = w$$

Now using a unit width,  $b=1$ , the area,  $A$  would be equal to  $bt = (1)t = t$  and the distributed load  $w$  would then be,  $w = pb = p$ , where  $p$  is the pressure. Substituting these parameters into the above equation yields,

$$p = \frac{8\sigma}{L^2} t \Delta \quad (3.5)$$

Next, a relationship between  $\Delta$  and  $\sigma$  is found through the constitutive relation of the material (stress-strain diagram).

The next step is to use compatibility to determine the relationship between strain and deflection. Once an exact strain is found, the corresponding stress can be determined from a stress-strain diagram. This produces pressure as a function of deflection (Static resistance function). This process is outlined next.

The first step of this process is to assume that strain is uniform along the length of the beam, it is known from the definition of strain that

$$L' = (1 + \varepsilon)(L) \quad (3.6)$$

Additionally, the arc length is given by

$$ArcLength = \int_0^L \sqrt{1 + (g'(x))^2}$$

where  $g'(x)$  may be replaced with  $y'$  from equation 3.3.

Now, let  $\beta = \frac{-8\Delta}{L^2}$ . Then the arc length may be written as

$$ArcLength = 2 \int_0^{\frac{L}{2}} \sqrt{1 + \beta^2 x^2} \quad (3.7)$$

Using integration tables,

$$\int \sqrt{x^2 + \alpha^2} = \frac{x\sqrt{x^2 + \alpha^2}}{2} + \frac{\alpha^2}{2} \ln(x + \sqrt{x^2 + \alpha^2}). \quad (3.8)$$

Next, the equation is manipulated to make the right side of Equation 3.7 similar in form to the left side of Equation 3.8. Since  $L'$  is the arc length, the following relation applies:

$$\begin{aligned} L' &= 2 \int_0^{\frac{L}{2}} \sqrt{1 + \beta^2 x^2} dx \\ &= 2 \int_0^{\frac{L}{2}} \beta \sqrt{\left(\frac{1}{\beta^2} + x^2\right)} dx \\ &= 2\beta \int_0^{\frac{L}{2}} \sqrt{\alpha^2 + x^2} dx \end{aligned}$$

where  $\alpha = \frac{1}{\beta^2}$ .

So, from substituting the above relationship for  $L'$  into Equation 3.8, it is seen that

$$L' = 2\beta \left[ \frac{x\sqrt{x^2 + \alpha^2}}{2} + \frac{\alpha^2}{2} \ln(x + \sqrt{x^2 + \alpha^2}) \right]_0^{\frac{L}{2}}$$

Solving the integral using the integration limits, and back-substituting the values for  $\alpha$  and  $\beta$  it is finally shown that

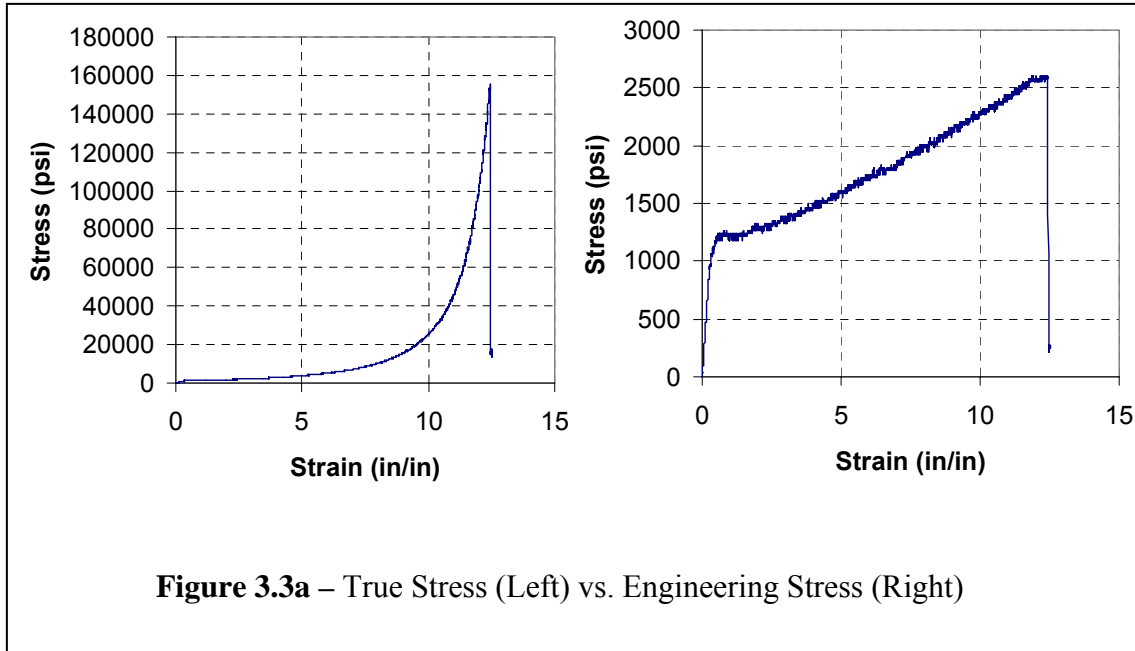
$$L' = 2 \left( \frac{-8\Delta}{L^2} \right) \left[ \frac{\frac{L}{2} \sqrt{\frac{L^2}{4} + \frac{L^4}{64\Delta^2}}}{2} + \frac{L^4}{128\Delta^2} \ln \left( \frac{L}{2} + \sqrt{\frac{L^2}{4} + \frac{L^4}{64\Delta^2}} \right) - \left( \frac{L^2}{16\Delta} + \frac{L^4}{128\Delta^2} \ln \left( \frac{L^2}{16\Delta} \right) \right) \right] \quad (3.9)$$

The following summarizes the remaining steps to determining the detailed analytical model:

1. Set  $\Delta$  equal to zero, and incrementally increase the value by a small amount
2. Use Equation 3.9 to determine the corresponding value for  $L'$
3. Use Equation 3.6 to calculate the strain
4. From the stress-strain curve, find the stress corresponding to the calculated strain
5. Use Equation 3.5 to calculate the pressure
6. Increment  $\Delta$  and start at step #2 again. Repeat process until the ductility limit is reached or failure in the polymer is predicted.
7. Plot the calculated pressures versus the incremented deflections

The analytical procedure described above is used to develop the resistance function of a polymer shown in Figure 3.3a. The true stress-strain relationship is used to develop the resistance for a 1/8-inch thick polymer sheet on a 12-ft high wall as shown in Figure 3.3b. Although Figure 3.3b indicates that the polymer could deflect up to 60 inches and provide a resistance of 4 psi before failure, other factors could produce failure and not allow the polymer to utilize its full ductility. Failures due to stress concentrations

at the connections and /or localized over stressed regions at mortar joints could control the resistance. Preliminary research (Beckman, 2005 and Bechtold, 2004) has indicated that these effects are critical, and additional research is needed to evaluate all failure limit states, other than ductility limit state, that could control the ultimate resistance of a blast retrofitted concrete wall using polymers.



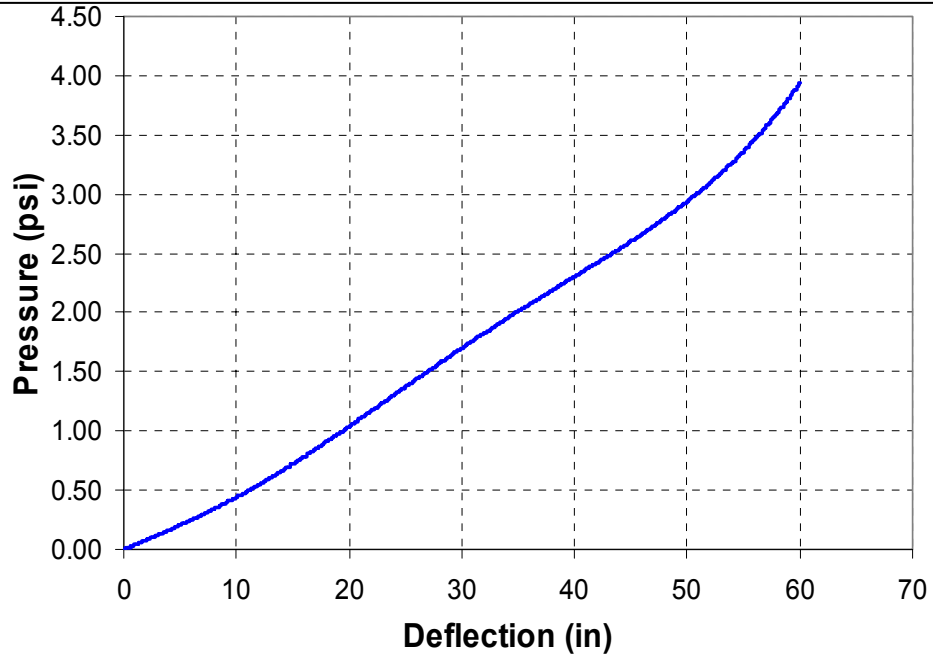


**Figure 3.3b** - Static Resistance Function of Polymer of Figure 3.3b

# CHAPTER 4 – EXPERIMENTAL EVALUATION

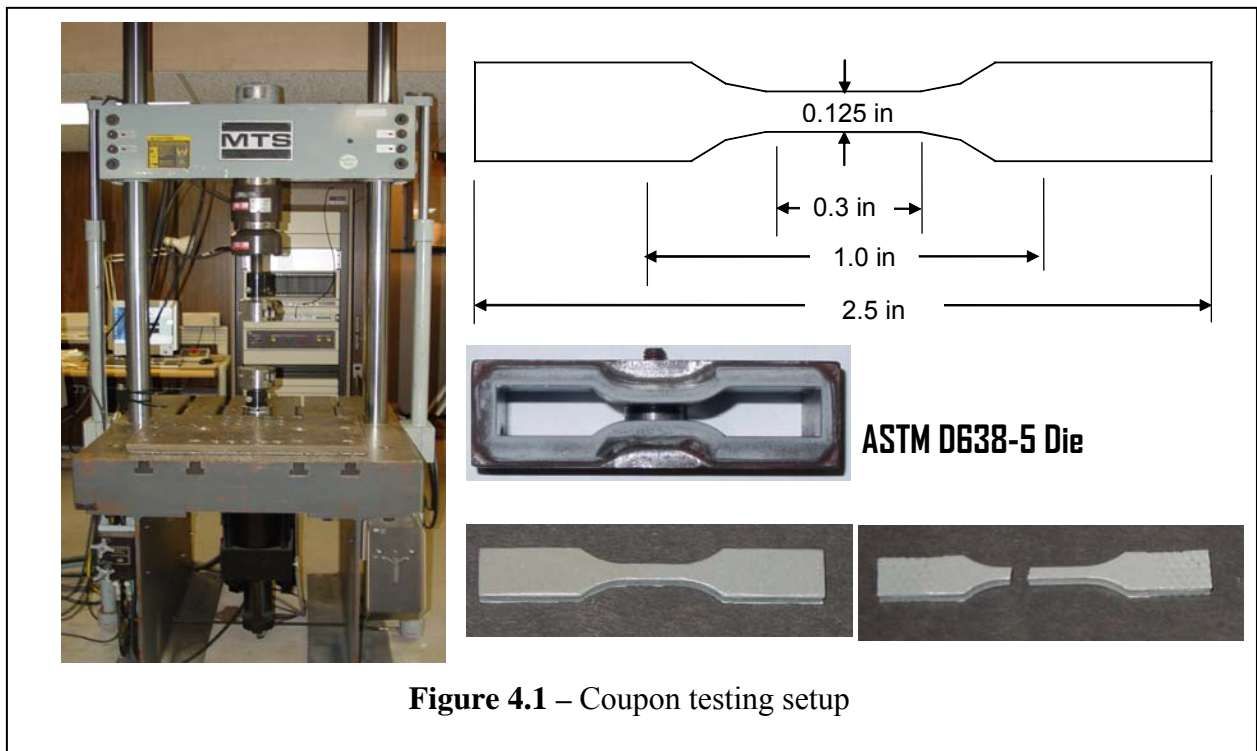
## 4.1 General

Once the analytical model for the static resistance function has been formulated, it is necessary to verify the model experimentally. To do this, three levels of experimental evaluations will be performed. Each test will help in verifying the predicted analytical model.

## 4.2 Coupon Testing

### 4.2.1 Setup and Procedure

The first set of tests ran was coupon testing. Coupons cut from the polymer sheets were tested under uniaxial tension to failure using a 2 inch per minute head speed. The coupons were tested following the ASTM D638 standard shown in Figure 4.1.

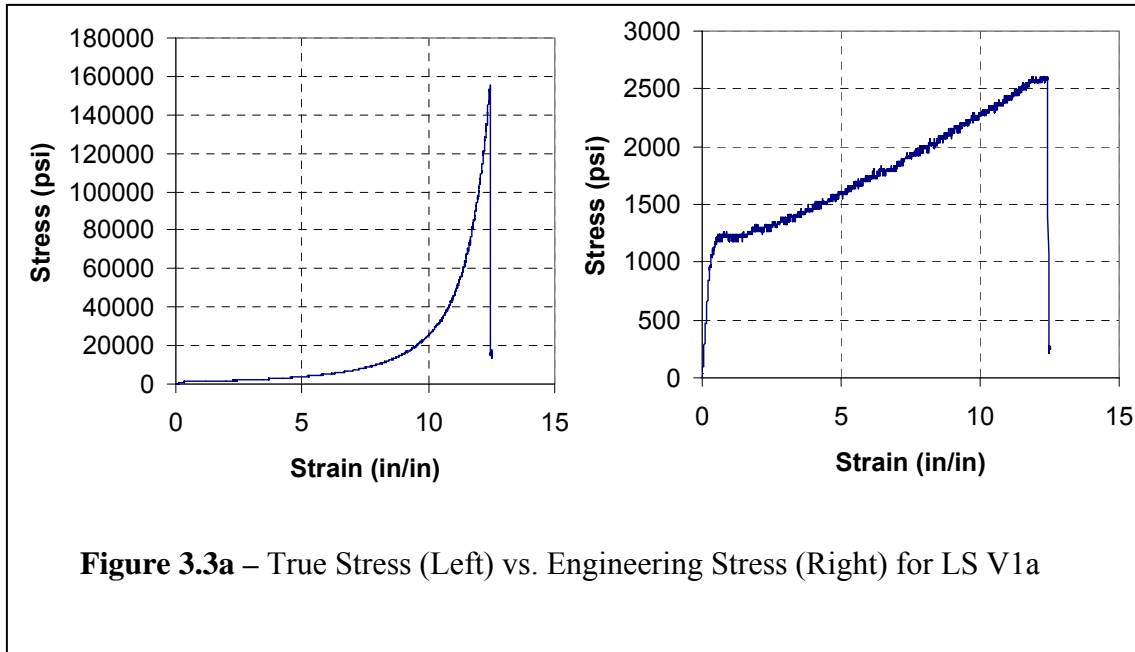




For this part of the study, there were a total of twelve coupons tested at AFRL, Tyndall AFB. Six of the coupons were cut longitudinally and six were cut transversely from the polymer sheet. This was done to ensure that the polymer is isotropic at all locations. Additionally, because the polymer's thickness varies, many coupons were needed to get an overall average for the sheet. Once the data was collected, the maximum tensile stress, elongation at the maximum tensile stress, the maximum elongation percentage, secant modulus, and toughness were calculated for the samples.

#### **4.2.2 Calculating True Stress from Engineering Stress**

The stress-strain diagrams produced throughout the testing depicts engineering stress and corresponding strain. Since during a blast, the polymer may undergo large deformations resulting in significant reduction of the original thickness of the samples. It is necessary to use true stress-strain relation instead of the engineering property. The difference between engineering stress and true stress is that engineering stress assumes there is no or very little reduction in area as when the specimen is loaded. This assumption works well for most civil engineering structures, because the structures are only allowed to deflect a very small amount. Under blast loading, there is a large amount of deflection and this assumption doesn't work well. For modeling the polymer sheets true stress will be used. Figure 4.2 shows a comparison between true and engineering stress for the LS V1a sample. From the figure it can be seen that as the load is increased the true stress begins to differ greatly with engineering stress. Similar calculations were done for each coupon.



#### **4.2.3 Results**

Figure 4.3 shows the engineering stress versus strain for all 12 coupons. Also, the maximum tensile stress, elongation at the maximum tensile stress, the maximum elongation percentage, secant modulus, and toughness are shown in Table 4.1.

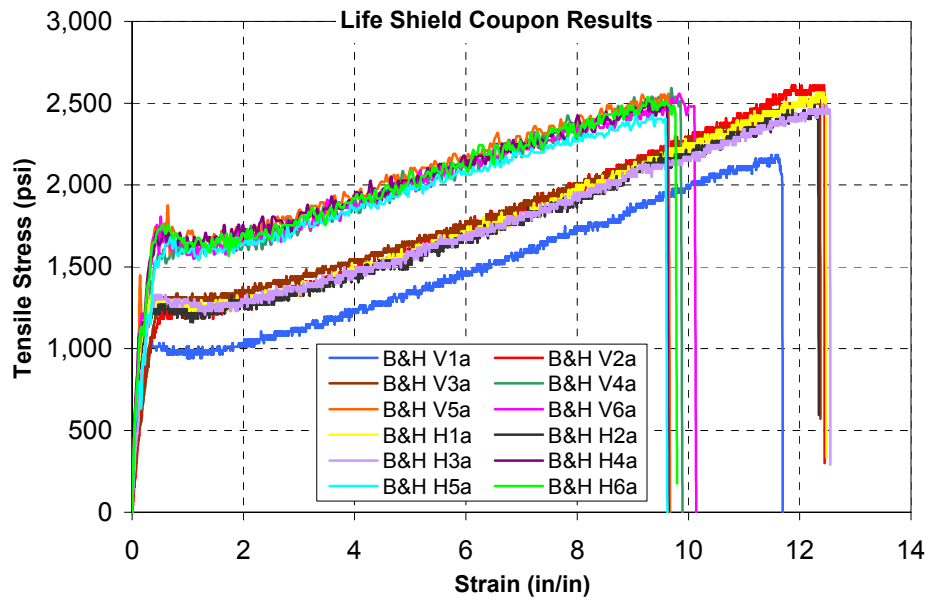


**Figure 4.3** - Stress-strain results of tensile tests on coupon samples

**Table 4.1** - Coupon test results for Life Shield (LS) samples

Sample Name	Maximum Tensile Strength psi	Elongation at Max. Tensile Strength %	Maximum Elongation %	Secant Modulus psi	Toughness psi*in/in
LS H1a	2,563	1229.05	1247.89	273	22,057
LS H2a	2,485	1226.29	1234.11	293	21,272
LS H3a	2,486	1241.23	1255.19	0	21,900
Mean	2,511	1232.19	1245.73	189	21,743
LS H4a	2,523	924.95	964.82	4,484	19,224
LS H5a	0	-0.17	962.18	3,464	18,449
LS H6a	2,538	926.61	979.76	4,451	19,545
Mean	1,687	617.13	968.92	4,133	19,073
LS V1a	2,183	1149.30	1169.30	234	17,190
LS V2a	2,608	1186.07	1244.96	280	22,110
LS V3a	2,542	1230.03	1237.27	327	22,163
Mean	2,444	1188.47	1217.18	280	20,488
LS V4a	2,593	969.47	989.35	3,392	19,545
LS V5a	2,551	917.08	967.18	4,243	19,544
LS V6a	2,557	983.72	1013.94	3,930	20,197
Mean	2,567	956.76	990.16	3,855	19,762
<b>Overall Mean</b>	<b>2,302</b>	<b>999</b>	<b>1,105</b>	<b>2,114</b>	<b>20,266</b>

#### **4.2.4 Summary and Conclusions**

Coupon testing is an important step in the determination of the constitutive relationship of the polymer sheets. It is very important to obtain ductility limits and maximum applied stresses to continue the development of the static resistance function. Additionally, values obtained from the stress-strain diagrams will be used in the dynamic modeling portion of the research. Next, the connection-level testing of the polymer is presented.

### **4.3 Connection Testing**

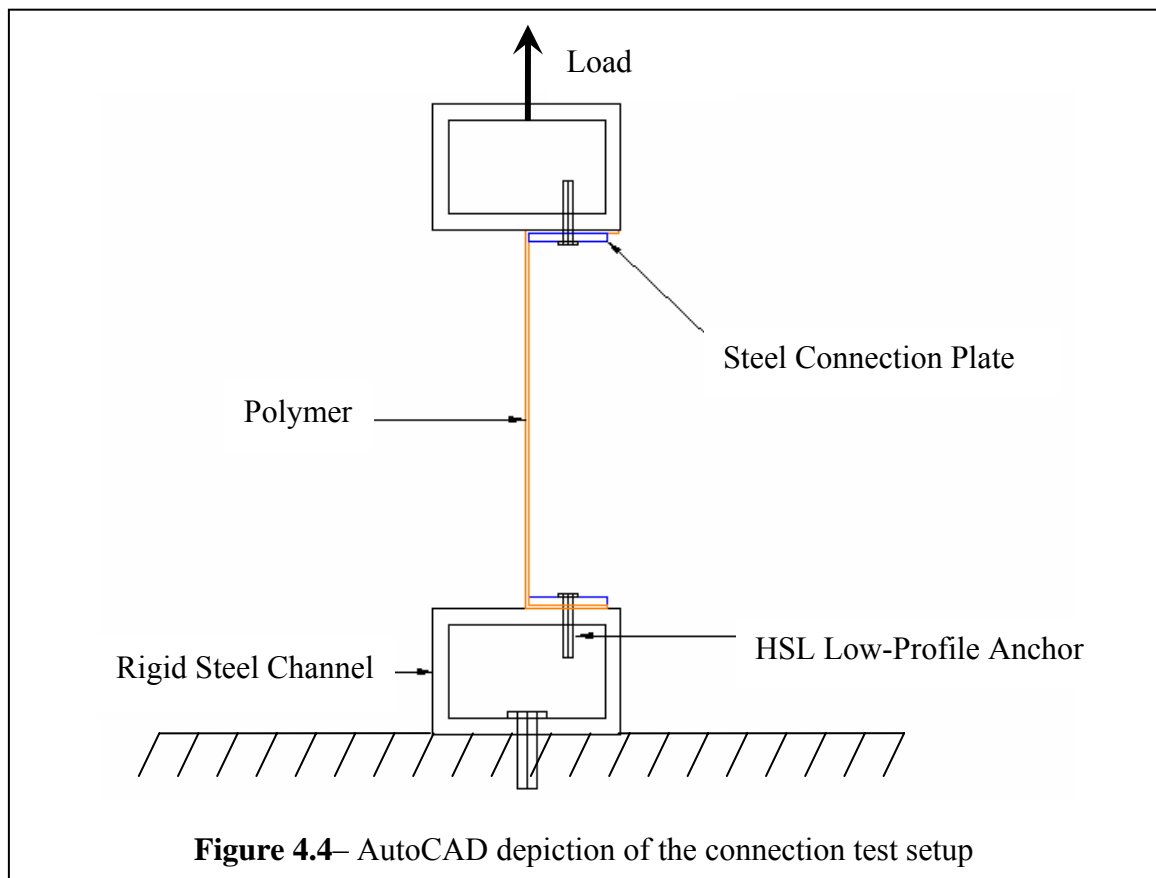
#### **4.3.1 General**

Polymers are capable of absorbing a great deal of energy which could make them a useful retrofit for CMU walls. One problem with using polymers is developing an effective connection method to allow them to utilize their full potential of high ductility. The most economical and installation-friendly way to connect the polymer is to bend the polymer and use a steel connection plate to bolt it to the floor and ceiling. This will increase the absorption capability of the CMU wall and reduce or eliminate fragments of the wall coming into the room. In order for the polymer to reach its full capacity, well-designed connection must be used to prevent premature failure at the floor and ceiling. To find the most effective and practical connection method, fifteen connection tests were performed using various bolt spacing and connection plate thicknesses. The bolt spacings used were 8, 12, and 16 inches and the connection plate thicknesses used were 0.125 inches and 0.25 inches.

### **4.3.2 Setup and Procedure**

In this section, a detailed description of the setup and procedure to achieve the most efficient connection method is provided.

The polymer samples were bent at a 90-degree angle and bolted between rigid channel and a steel connection plate. The length of the bent between the channel and the plate was 6 inches and the bolts were centered on the plate 3 inches from each side. The top channel was connected to an MTS machine that loaded the polymer sample in tension. This setup is illustrated in Figure 4.4.



The polymer was to be tested using 2 thicknesses, which were 0.125 inches and 0.16 inches. Additionally, the bolt spacing and the steel connection plate thickness would

also be varied. There would be 3 different bolt spacings of 8, 12, and 16 inches, and 2 connection plate thicknesses of 0.125 and 0.25 inches. After several tests were completed, it was decided that the length of the samples should be reduced from 24” to 6” in order to try to fail the samples since the travel on the MTS machine is limited. The width remained a constant 36 inches and each bolt was torqued to 1600 lb-in.

With regard to applied torque on the bolts, Hilti Anchors are commonly used in the field, and the HSL low-profile heavy-duty sleeve anchors apply a uniform torque of 1600 lb-in to each bolt. The bolts used to attach the polymer were 5/8” high-strength bolts. A picture of the actual set-up can be seen in Figure 4.5. Failure was sudden, and could have initiated at either of the edges where the steel plate might have “cut” into the polymer sample.



**Figure 4.5** - Picture of the connection setup

Once the polymer was in place, the MTS machine then loaded the sample. Due to the high deflection limits of the polymer, the MTS machine ran out of travel before failing any of the samples. Despite this, sufficient data was collected and optimal spacing and connection plate thicknesses were obtained. Recently, a very short sample was tested to failure to ensure that no significant response characteristics are missed in the samples that were not failed. The sample tested showed no significant response characteristics before failing. The polymer tore in a jagged manner mainly in the gage length. Figure 4.6 shows the polymer after the test. Failure was sudden, and could have initiated at either of the edges where the steel plate might have “cut” into the polymer sample.



**Figure 4.6** – Failure of Polymer Sample

### **4.3.3 Results**

In order to test all parameters to develop the most optimal design, a connection test matrix was developed for the connection experiments. Table 4.2 shows the results of the 16 tests performed to develop the most effective connection. Figures 4.7 -4.35 show the test setup of all 17 samples and their response during various stages of the tests. These Figures also show the load –displacement response of all samples

**Table 4.2 – Results from Connection Testing**

<b>Sample #</b>	<b>Test sample name</b>	<b>Sample length, <math>L</math> (in)</b>	<b>Sample thickness, <math>t</math> (in)</b>	<b>Clamping plate thickness, <math>t_p</math> (in)</b>	<b>Anchor spacing, <math>s</math> (in)</b>	<b>Energy absorbed (lb-in)</b>
1	LS-C1b	18	0.125	0.125	12	24,780
2	LS-C2	36	0.125	0.25	12	19,893
3	LS-C2b	18	0.125	0.25	12	27,296
4	LS-C3	36	0.125	0.125	8	13,506
5**	LS-C3**	36	0.125	0.125	8	17,428
6	LS-C3b	18	0.125	0.125	8	25,593
7	LS-C4b	18	0.125	0.25	8	27,847
8	LS-C5	36	0.160	0.125	12	23,143
9	LS-C5b	18	0.160	0.125	12	30,804
10	LS-C6	36	0.160	0.25	12	27,641
11	LS-C6b	18	0.160	0.25	12	32,840
12	LS-C7b	18	0.160	0.125	8	17,717
13	LS-C8	36	0.160	0.25	8	20,212
14	LS-C8b	18	0.160	0.25	8	43,541
15	LS-C9	18	0.125	0.125	16	24,461
16	LS-C10	18	0.160	0.125	16	34,632

\*\* Test repeated twice



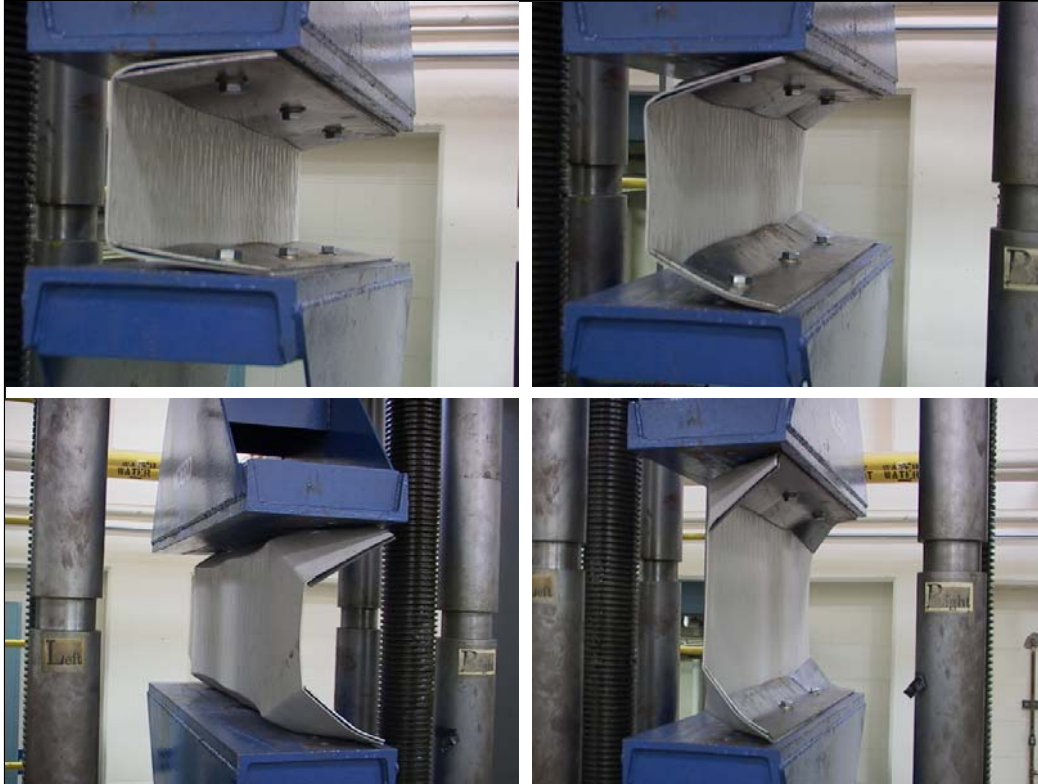


**Figure 4.7 - Test sample LS-C1b**

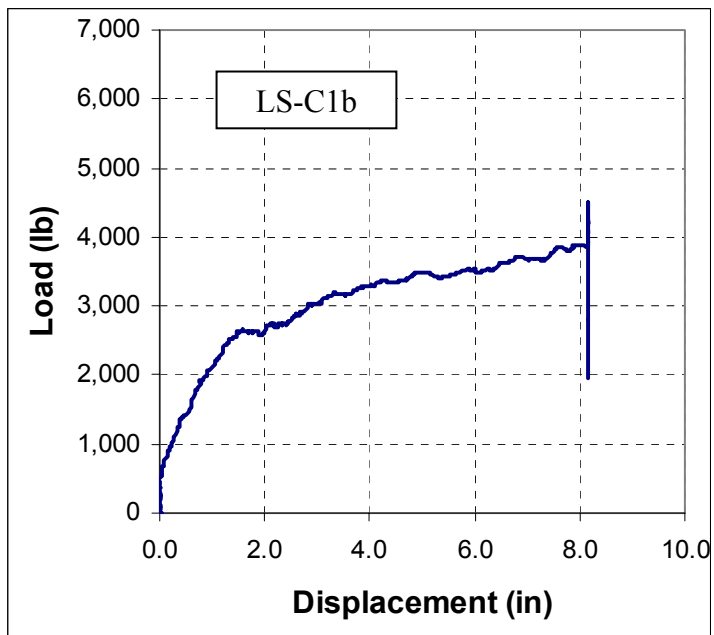


**Figure 4.8 - Load-deflection curve for LS-C1b**



**Figure 4.9 - Test sample LS-C2**

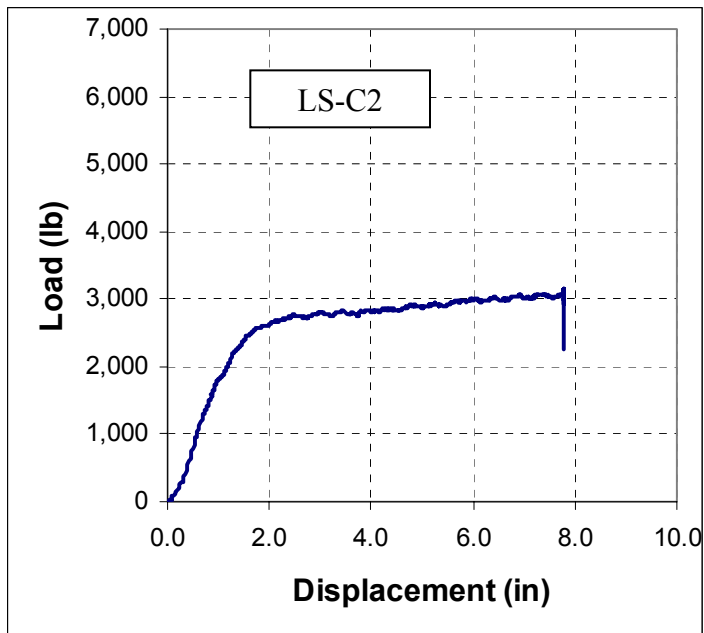


**Figure 4.10 - Load-deflection curve for LS-C2**



**Figure 4.11 - Test sample LS-C2b**

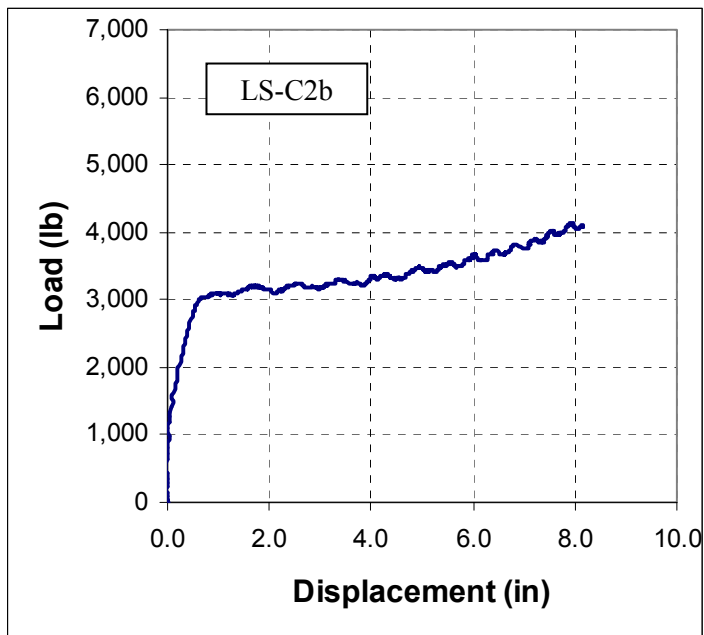


**Figure 4.12 - Load-deflection curve for LS-C2b**



**Figure 4.13 - Test sample LS-C3**

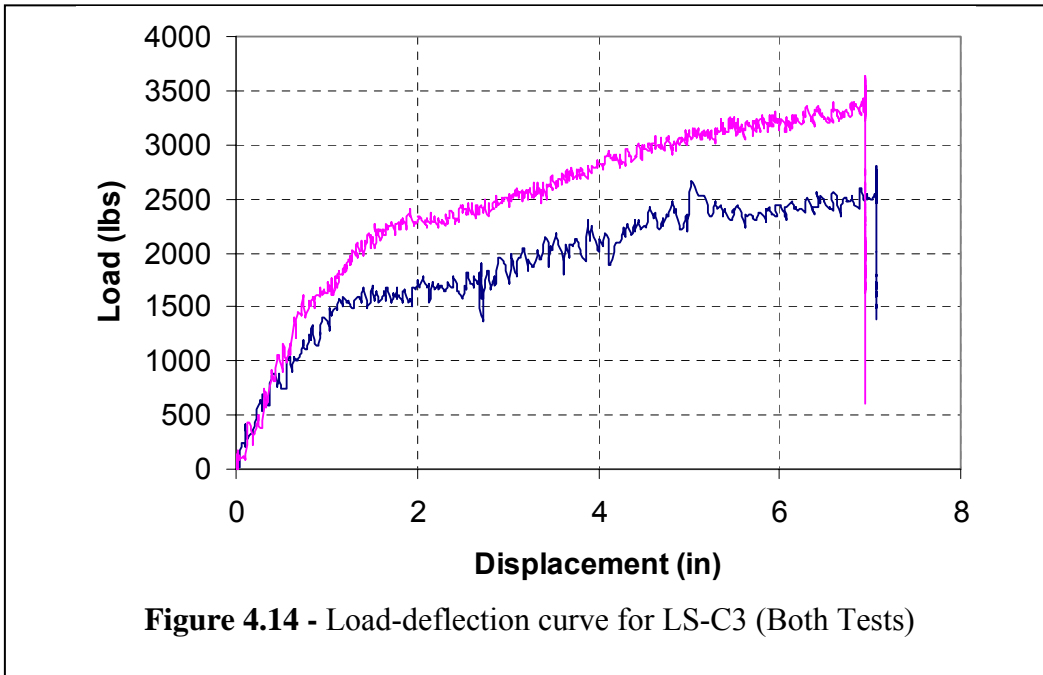


**Figure 4.14 - Load-deflection curve for LS-C3 (Both Tests)**



Figure 4.15 - Test sample LS-C3b

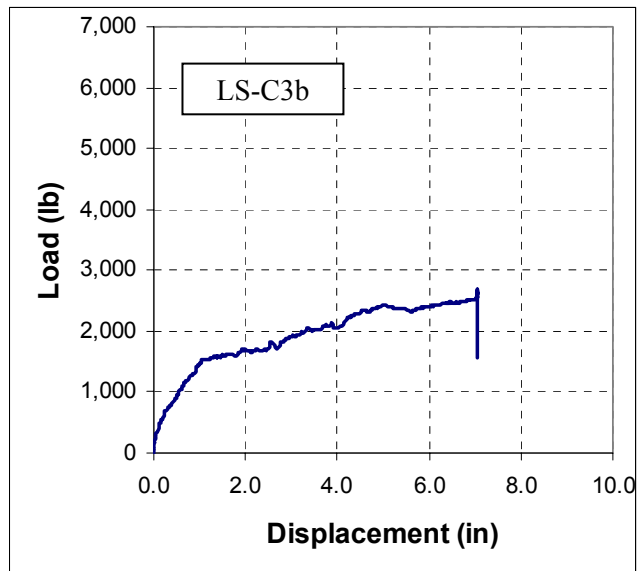
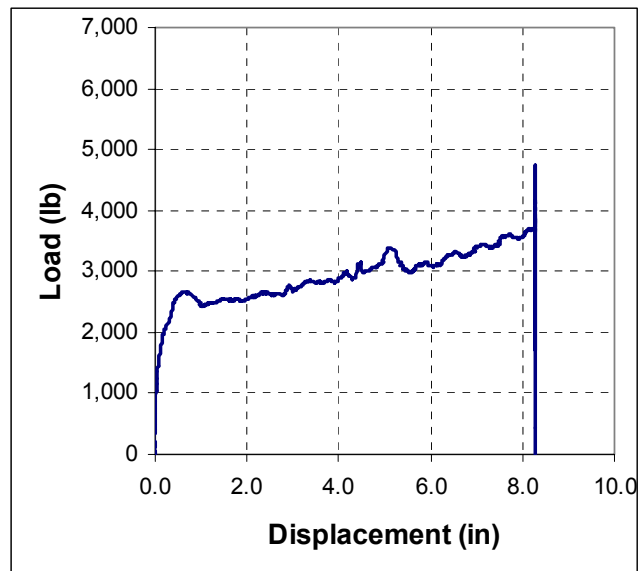


Figure 4.16 - Load-deflection curve for LS-C3b



**Figure 4.17 - Test sample LS-C4b**



**Figure 4.18 - Load-deflection curve for LS-C4b**

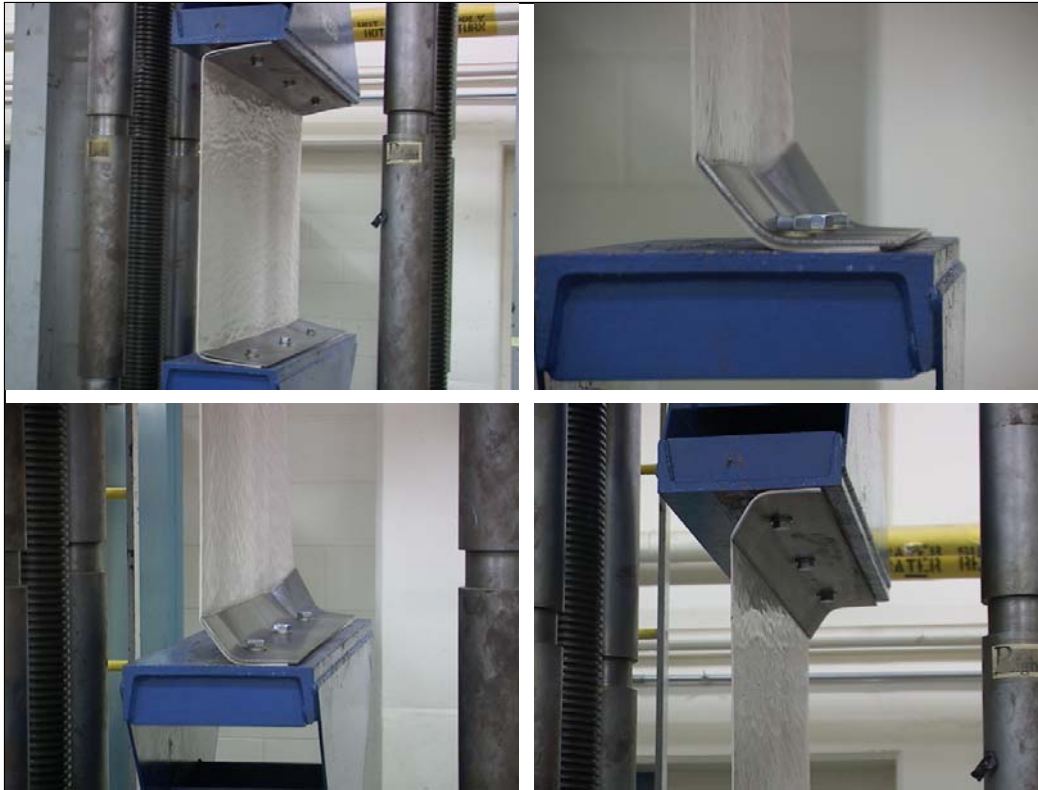


**Figure 4.19 - Test sample LS-C5**

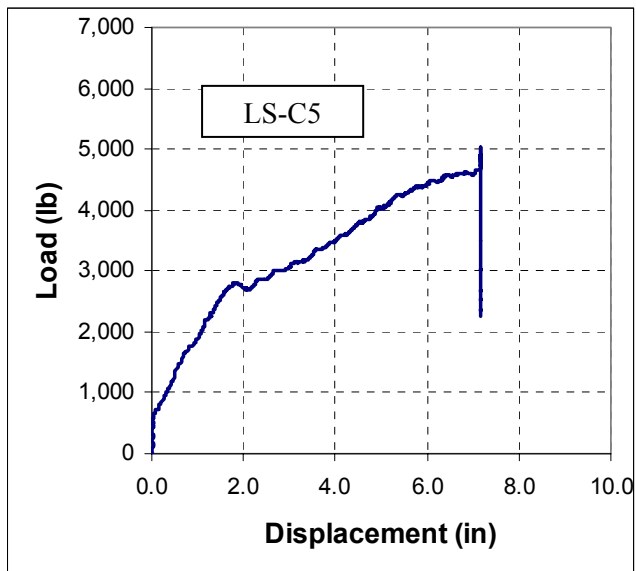


**Figure 4.20 - Load-deflection curve for LS-C5**

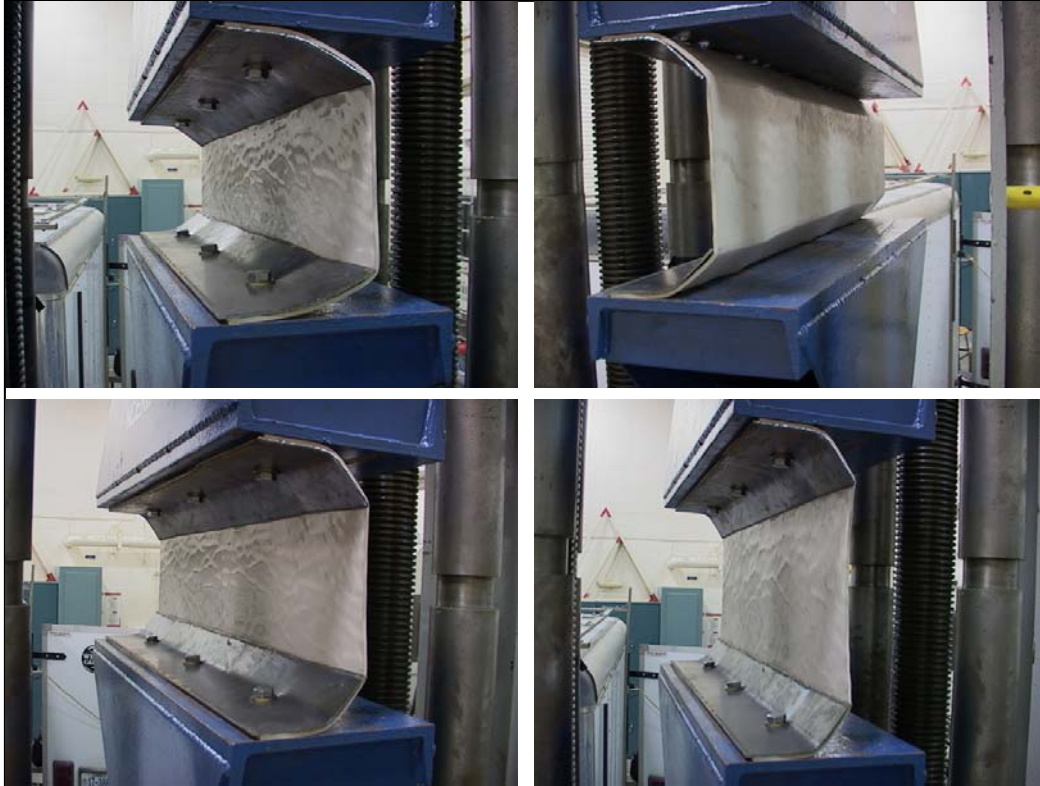


**Figure 4.21 - Test sample LS-C5b**

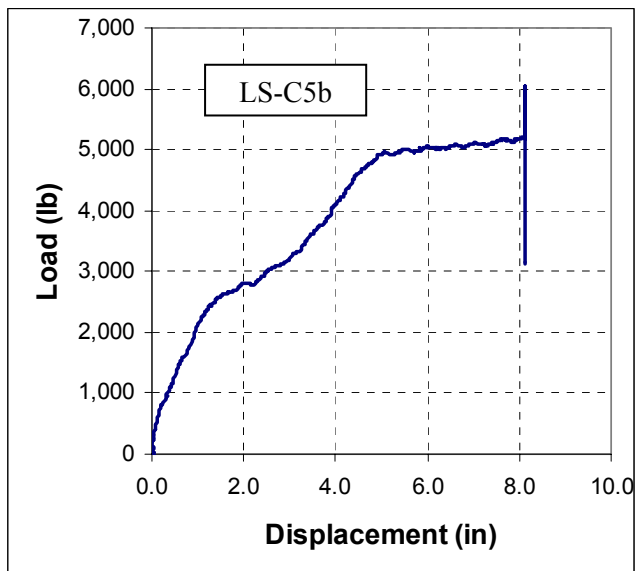


**Figure 4.22 - Load-deflection curve for LS-C5b**





**Figure 4.23 - Test sample LS-C6**

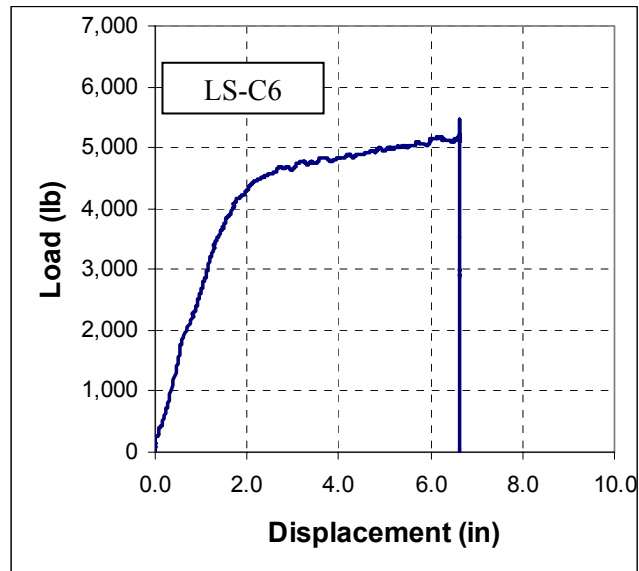


**Figure 4.24 - Load-deflection curve for LS-C6**



**Figure 4.25 - Test sample LS-C6b**

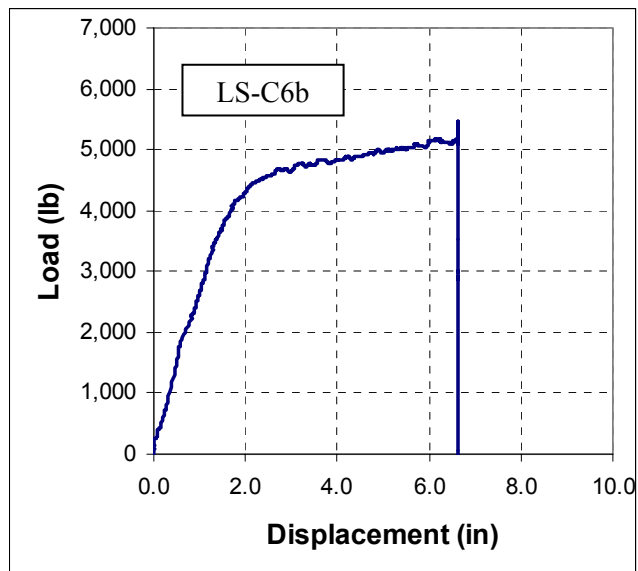


**Figure 4.26 - Load-deflection curve for LS-C6b**



**Figure 4.27 - Test sample LS-C7b**

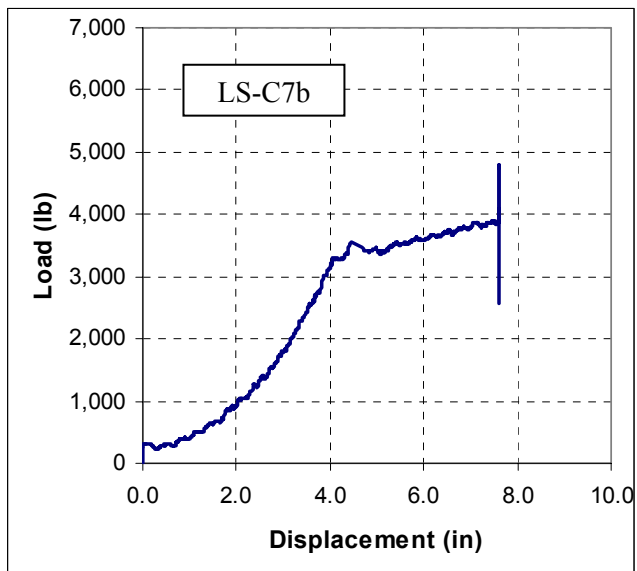


**Figure 4.28 - Load-deflection curve for LS-C7b**



**Figure 4.29 - Test sample LS-C8**

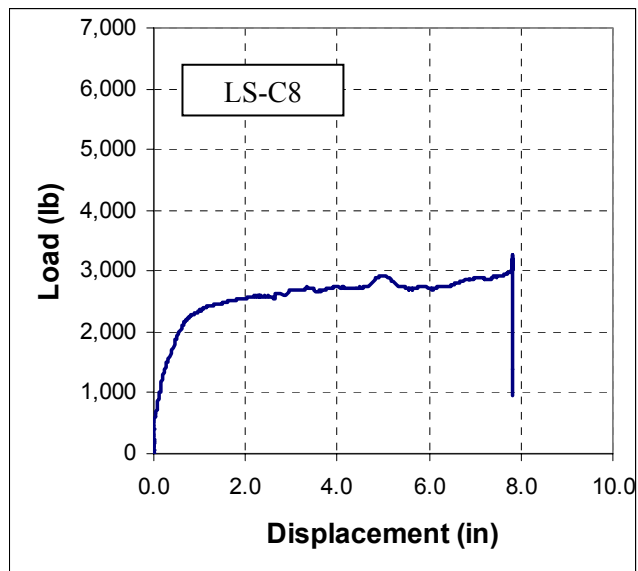


**Figure 4.30 - Load-deflection curve for LS-C8**



**Figure 4.31 - Test sample LS-C8b**

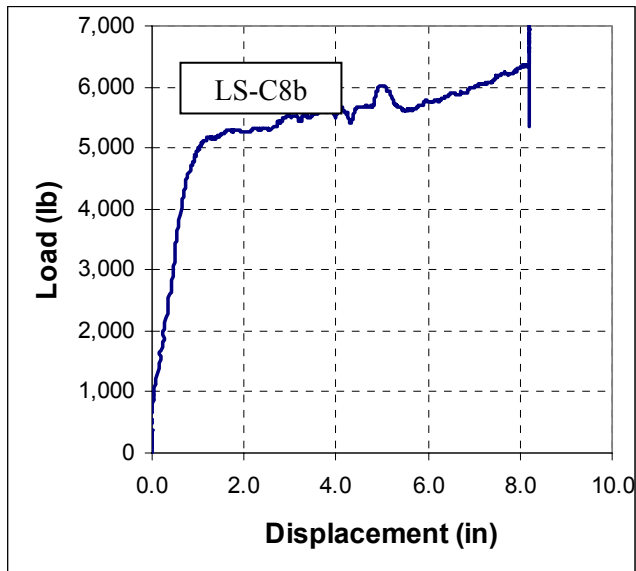


**Figure 4.32 - Load-deflection curve for LS-C8b**



**Figure 4.33 - Test sample LS-C9**

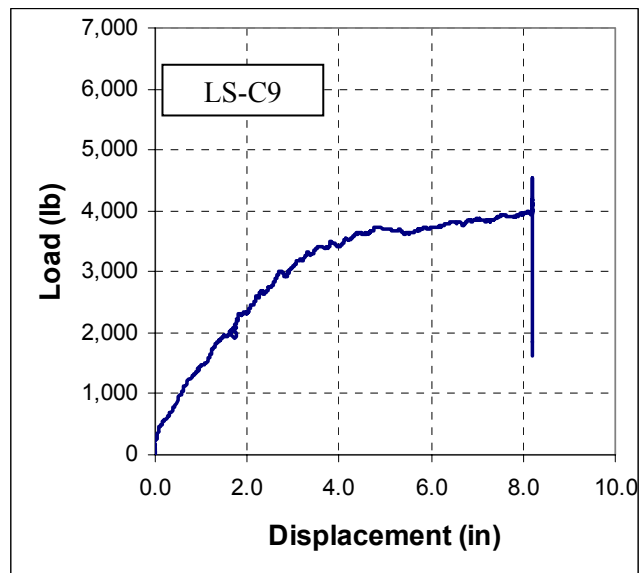


**Figure 4.34 - Load-deflection curve for LS-C9**



**Figure 4.35 - Test sample LS-C10**

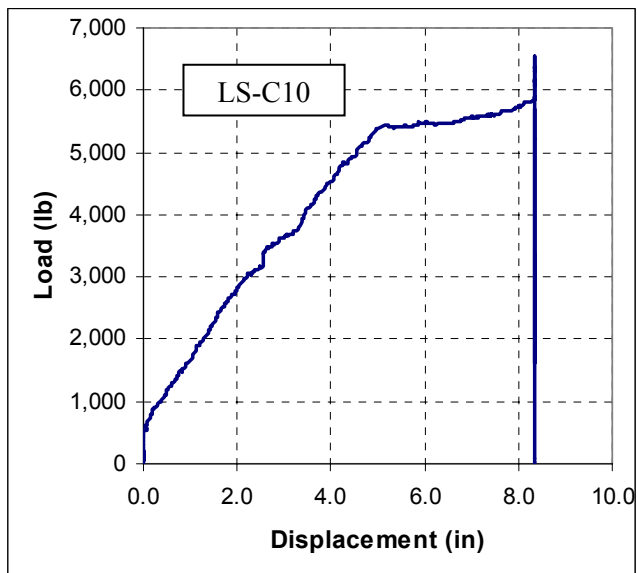


**Figure 4.36 - Load-deflection curve for LS-C10**

#### **4.3.4 Summary and Conclusions**

After analyzing the data, it can be seen that by choosing certain parameters, the polymer sheet will be allowed to develop most of its full capacity. One of the main reasons for running connection tests is to find how thick of a connection plate should be used in order for the polymer to not tear out at the bolts causing premature failure. From observations during the tests and from the pictures it can be seen that a 1/4" connection plate should be used to provide enough clamping resistance to prevent tear out at the connection. From observing the tests using the 1/8" connection plate thickness, it was seen that the plate deformed upward. In some retrofitted systems, bending of the plate can add ductility which in turn would cause greater energy absorption capability of the system. But for this retrofit system, there is plenty of ductility provided by the polymer. Besides, this would cause the polymer to tear out from the bolt holes in the polymer sheet which would cause premature failure.

The next parameter that was varied during the tests was the bolt spacing. There were three spacing chosen for the test which were 8", 12", and 16". The idea was to see how far the bolts could be spaced without losing energy absorption or allow the connection plate to bend causing the polymer to tear out at the connection. It was found that a 16" spacing was the optimal spacing for the bolts. It was also seen that a 12" spacing works good too, so it was decided that both spacings should be used in the component testing (Section 4.3).

The final parameter that was varied was the thickness of the polymer. The polymer had two thicknesses, 0.125" and 0.160". For most of the tests, the energy



absorption was much greater using the 0.160" sample thickness. For the component beam tests both the 0.125" and 0.160" thicknesses will be evaluated.

These tests show that by finding the right combination of parameters, the energy absorption capabilities of the polymer sheets can be increased greatly. This is because the polymer sheets are allowed to reach their full capacity. It is the recommendation of this research that ¼" connection plate and 16" bolt spacing be used for optimum energy absorption.

One note should be made about an observation that was seen about how the connection plate edges could reduce the strength of the polymer if there were sharp edges present. In these tests, the polymer sheets were not extended beyond the plate end, preventing the corner of the plate from tearing into the polymer. It is expected that a sharp corner could significantly reduce the polymer tear strength. Such results of this premature failure were observed in steel sheet retrofit system (Kennedy, 2005). The sharp edges reduced the tensile capacity of the steel sheets by more than 50%. As a result, this should be avoided to prevent premature tearing of the polymer sheets.

Additionally, a table was made comparing the max theoretical load to the experimental load obtained from the connection test (Table 4.3). From the table, several observations can be made. All of the samples with the shorter gage length utilized more of its theoretical capacity compared with the sample with identical parameter except gage length. This is because the shorter samples were loaded closer to failure than the longer samples. The sample that produced the highest percent capacity was LS-C8b. This sample had a gage length of 6 inches, a thickness of 0.160 inches, used a clamping plate thickness of 0.25 inches, and anchor spacing of 8 inches.

**Table 4.3-** Theoretical Capacity Compared with Experimental Capacity

Sample Name	Theoretical Capacity	Experimental Capacity	
	P <sub>max</sub> (kip)	P <sub>max</sub> (kip)	% of Capacity
LS-C1b	10.35	3.88	37.49
LS-C2	10.35	3.05	29.47
LS-C2b	10.35	4.1	39.61
LS-C3	10.35	2.45	23.67
LS-C3**	10.35	3.32	32.08
LS-C4b	10.35	3.72	35.94
LS-C5	13.248	4.61	34.80
LS-C5b	13.248	5.17	39.02
LS-C6	13.248	5.04	38.04
LS-C6b	13.248	5.24	39.55
LS-C7b	13.248	3.87	29.21
LS-C8	13.248	2.98	22.49
LS-C8b	13.248	6.35	47.93
LS-C9	10.35	3.94	38.07
LS-C10	13.248	5.73	43.25

## **4.4 Component Beam Testing**

### **4.4.1 General**

The final level of testing is the component beam test. The component beams will be subjected to a uniform static loading and using the optimal connections obtained from the connection tests. Once tested, the results will be compared to the analytical model predicted in Chapter 3.

### **4.4.2 Setup and Procedure**

The component beam tests are polymer sheets cut 11 feet long and 22 inches wide, however with the 6 inches that is bent on each side the gage length of the sample becomes 10 feet. There will be two thicknesses tested which are 0.125 inches and 0.16 inches. For all tests, a ¼ inch connection plate will be used. Two bolt spacing of 12 and 16 inches were tested. The testing matrix is shown in Table 4.3. The samples were

tested using a 16-point loading tree closely simulating a uniform load on the sheets. An AutoCAD drawing of the 16-point loading tree is shown in Figure 4.36a. Figure 4.36b shows test polymer sample in the 16-point loading tree at the beginning of the test. Figure 4.36c shows the polymer nearing the end of the test. The mechanical connection at the beginning and during the test is shown in Figure 4.36d.

**Table 4.4 - Component Beam Test Matrix**

Test #	Sample Name	Sample thickness, t (in)	Connection plate thickness, $t_p$ (in)	Hole Spacing, s (in)	Sample Size (in)
1	LS-T1	0.125	0.25	12	22x120
2	LS-T2	0.125	0.25	16	22x120
3	LS-T3	0.160	0.25	12	22x120
4	LS-T4	0.160	0.25	16	22x120

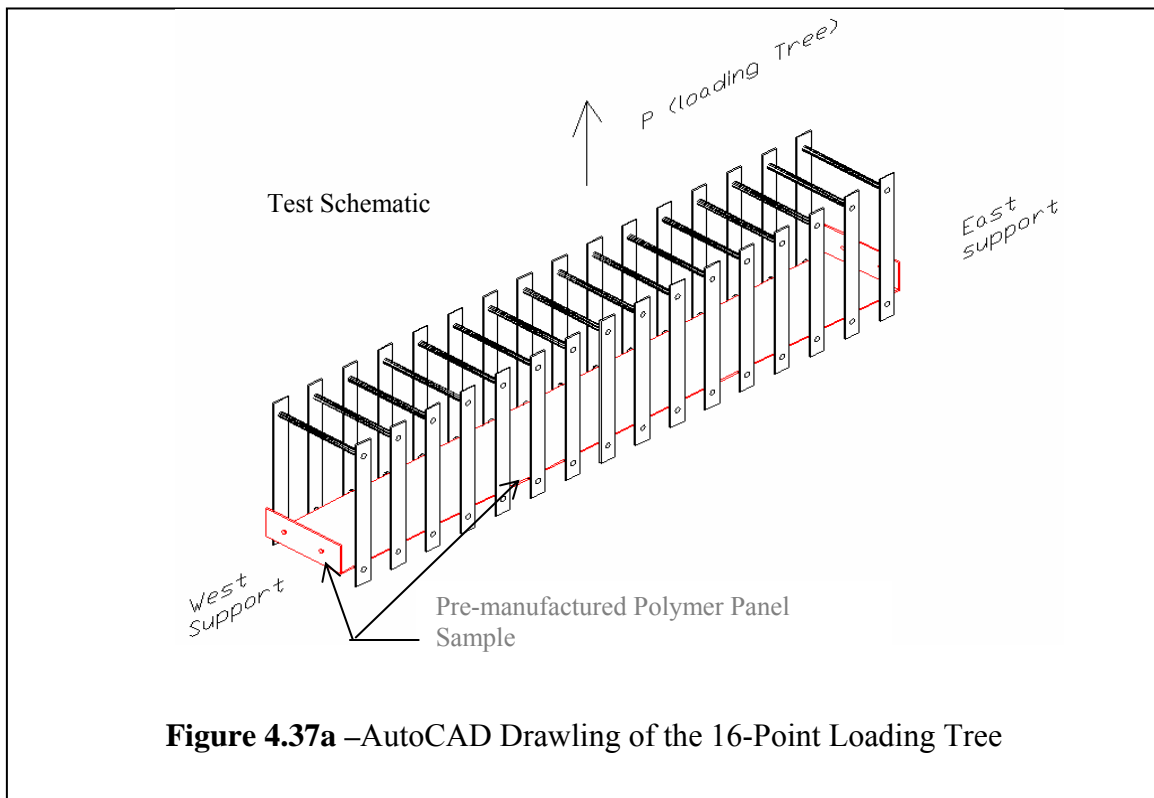


**Figure 4.37a –AutoCAD Drawing of the 16-Point Loading Tree**



**Figure 4.37b** –Polymer Sample at the Beginning of the Test



**Figure 4.37c** –Polymer Sample Nearing the End of the Test

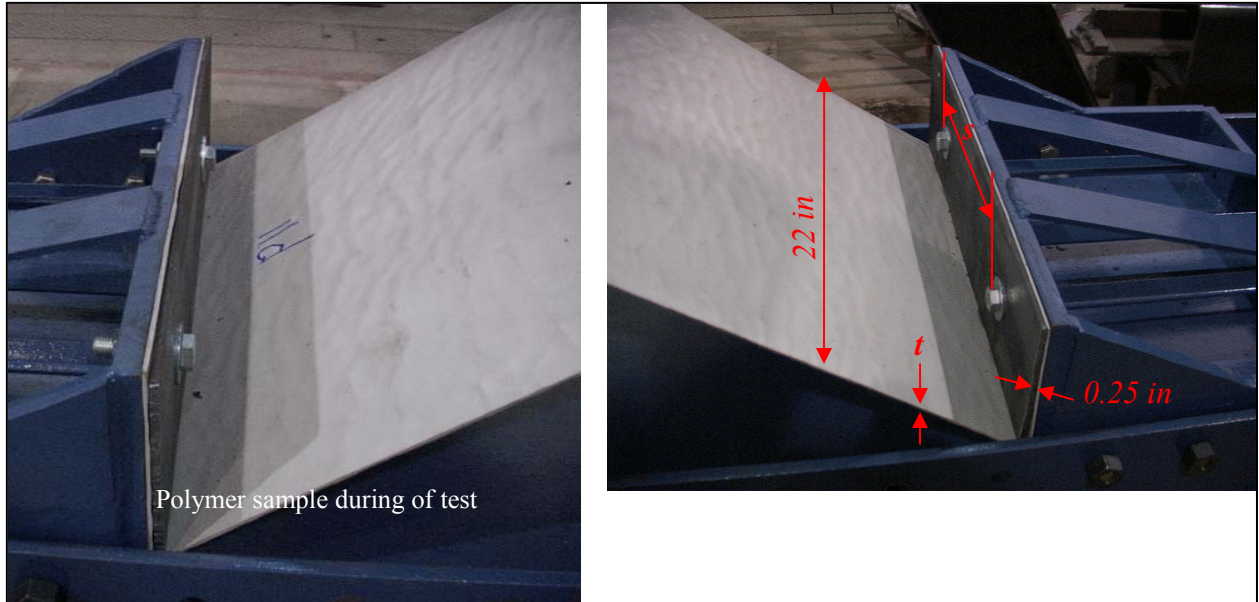
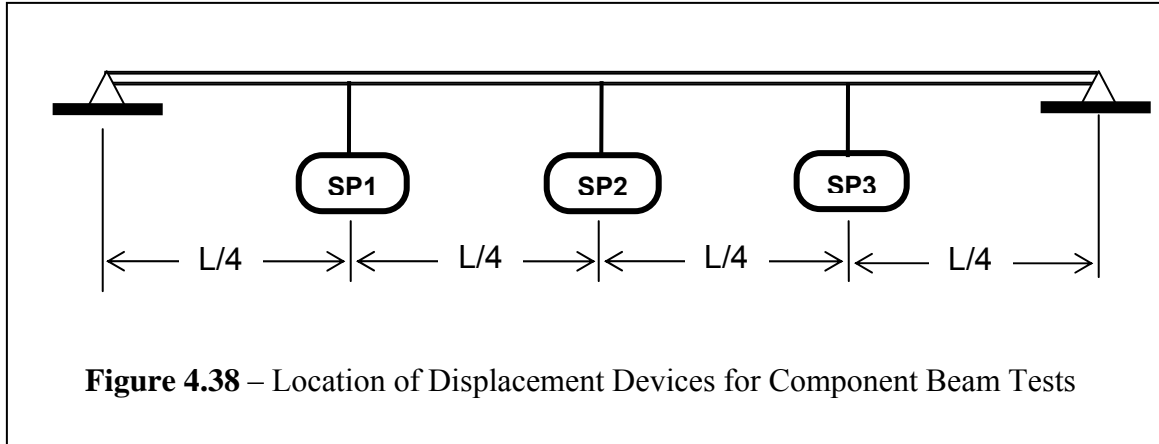


**Figure 4.37d** – Connection at the Beginning (Left) and During the Test (Right)

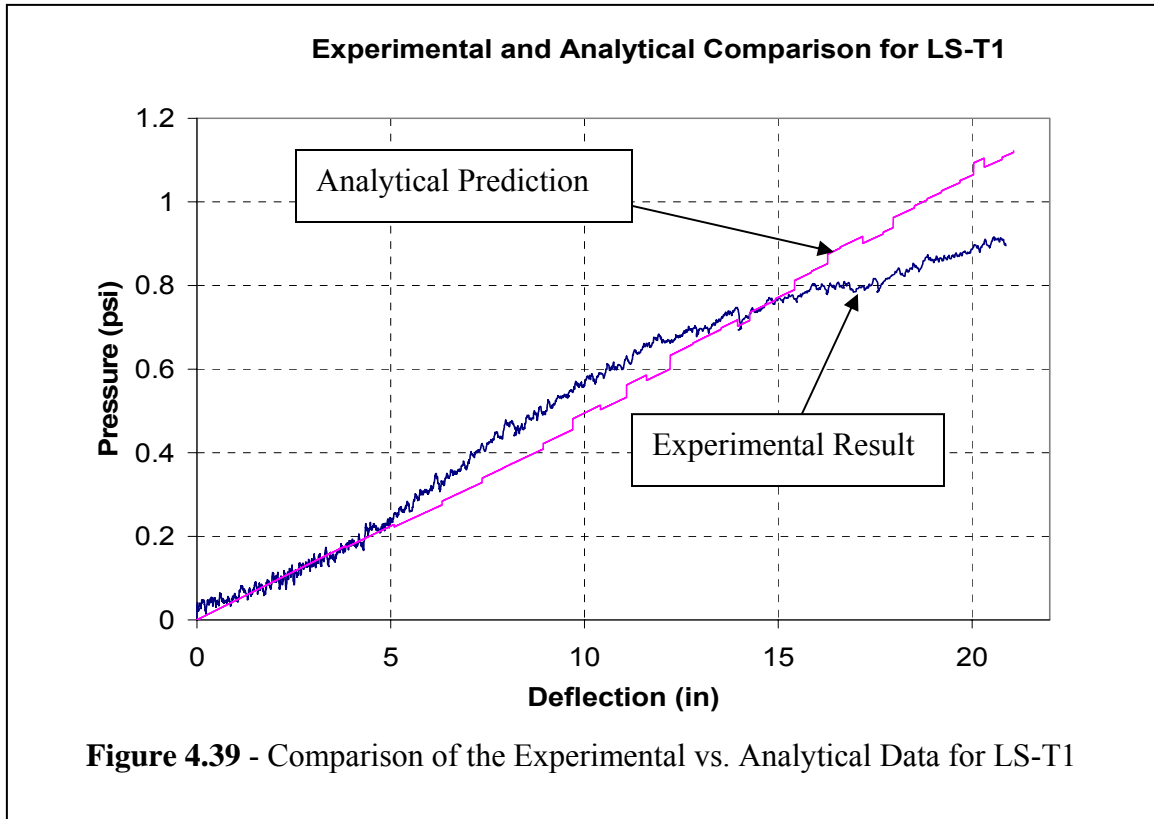
During the tests, the load-deflection data were recorded using a loading cell and three spring potentiometers. The potentiometers were placed at quarter points along the sample (Figure 4.37). The potentiometers and loading cell were connected to LabView, where load and deflection were recorded. Once the load and deflection was collected, it was used to calculate the equivalent pressure-displacement response (Static Resistance Function) of the blast mitigation system, which is then compared to the analytical model of the static resistance.



### **4.4.3 Results**

#### *Component test LS-T1:*

Sample LS-T1 had a thickness of 0.125 and used a 12 inch bolt spacing for the connections. Due to the loading cell having a maximum deflection of 20 inches, the polymer sheet never reached failure. However, there was enough data to compare to the analytically predicted model. To predict the model, stress-strain relations attained from coupon testing was used. The comparison of the experimental data recorded from LS-T1 and the analytical model is shown in Figure 4.38.



*Component test LS-T2:*

Sample LS-T1 had a thickness of 0.125 and used a 16 inch bolt spacing for the connections. Due to the loading cell having a maximum deflection of 20 inches the polymer sheet never reached failure. However, there was enough data to compare to the analytically predicted model. To predict the model, stress-strain relations attained from coupon testing was used. The comparison of the experimental data recorded from LS-T2 and the analytical model is shown in Figure 4.39.

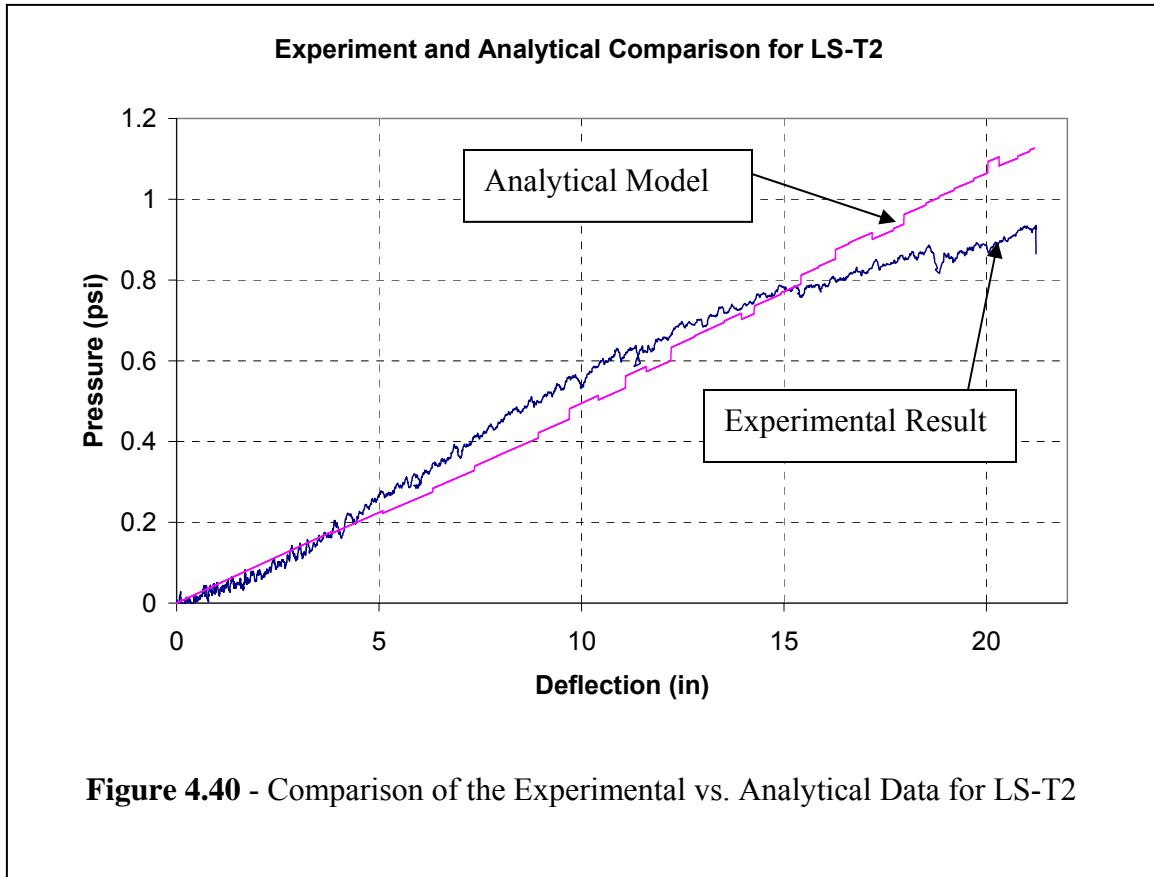
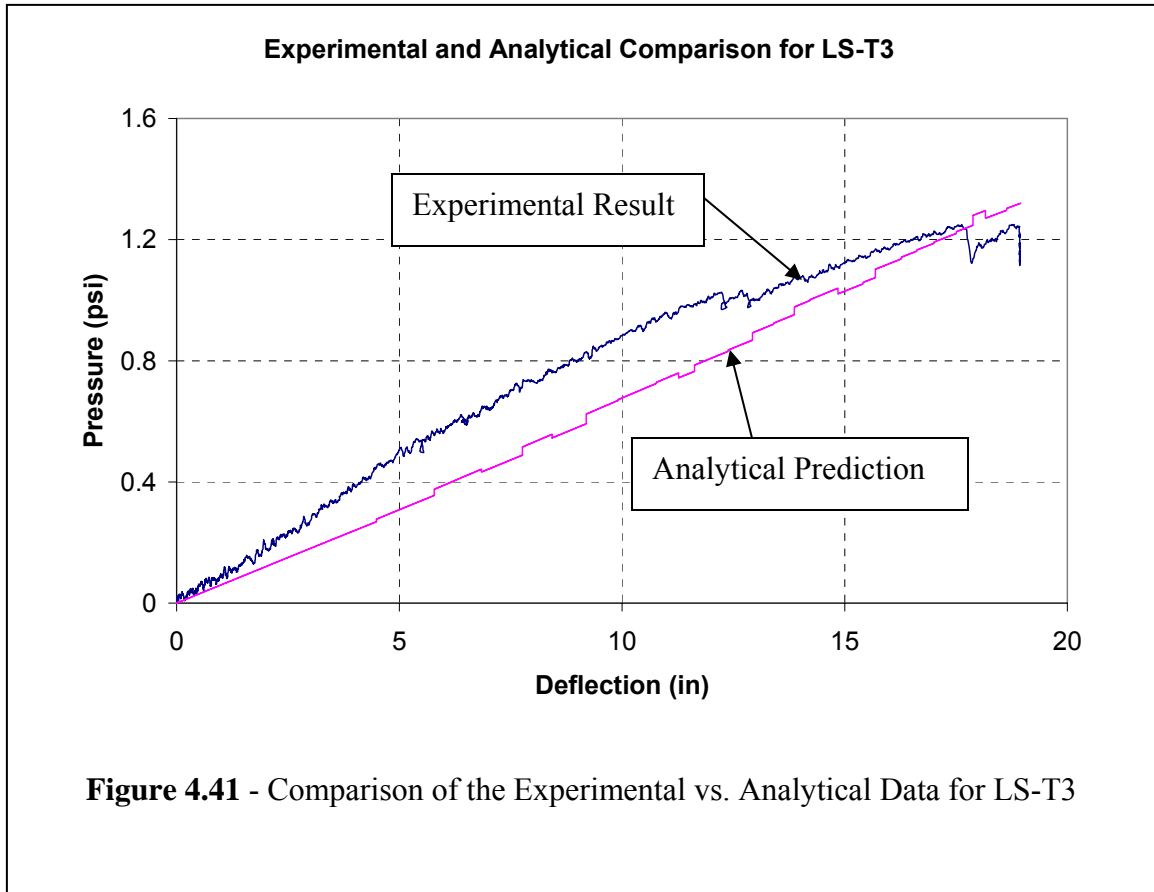


**Figure 4.40** - Comparison of the Experimental vs. Analytical Data for LS-T2

*Component test LS-T3:*

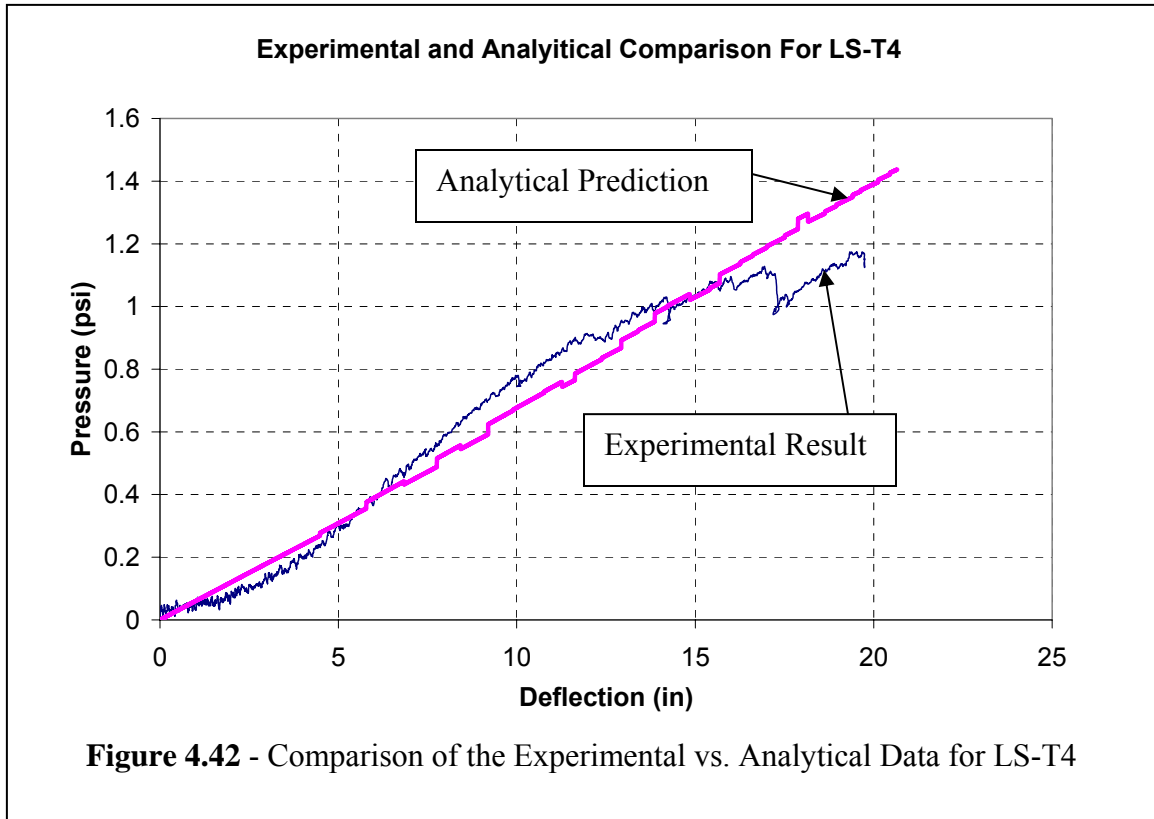
Sample LS-T1 had a thickness of 0.16 and used a 12 inch bolt spacing for the connections. Due to the loading cell having a maximum deflection of 20 inches the polymer sheet never reached failure. However, there was enough data to compare to the analytically predicted model. To predict the model, stress-strain relations attained from coupon testing was used. The comparison of the experimental data recorded from LS-T3 and the analytical model is shown in Figure 4.40.





*Component test LS-T4:*

Sample LS-T4 had a thickness of 0.16 and used a 16 inch bolt spacing for the connections. Due to the loading cell having a maximum deflection of 20 inches the polymer sheet never reached failure. However, there was enough data to compare to the analytically predicted model. To predict the model, stress-strain relations attained from coupon testing was used. The comparison of the experimental data recorded from LS-T4 and the analytical model is shown in Figure 4.41.



#### 4.4.4 Summary and Conclusion

From each of the comparisons, it can be seen that the analytical model predicted the behavior of the polymer sheets very well. It can also be seen that by increasing the bolt spacing to 16 inches, resulted in no energy absorption loss. For this reason it is recommended to use the 16 inch bolt spacing for design. Additionally, by increasing the thickness of the polymer from 0.125 inches to 0.16 inches, the polymer was able to absorb much more energy. However, from the comparisons, the analytical model predicted the smaller thicknesses much better than the larger thicknesses. More testing of larger thicknesses should be performed in order to see if this trend continues for thicker polymers.

From the graphs it can be seen that the model predicts the data very well at low deflections and then begins to become less accurate. This can be attributed to a couple of

factors, which include the tree's 16 loading points begin to slip at high deflections due to the angle it begins to make with the polymer sheets. Second, the loading points become less orthogonal with the polymer.

# CHAPTER 5 –DYNAMIC MODELING

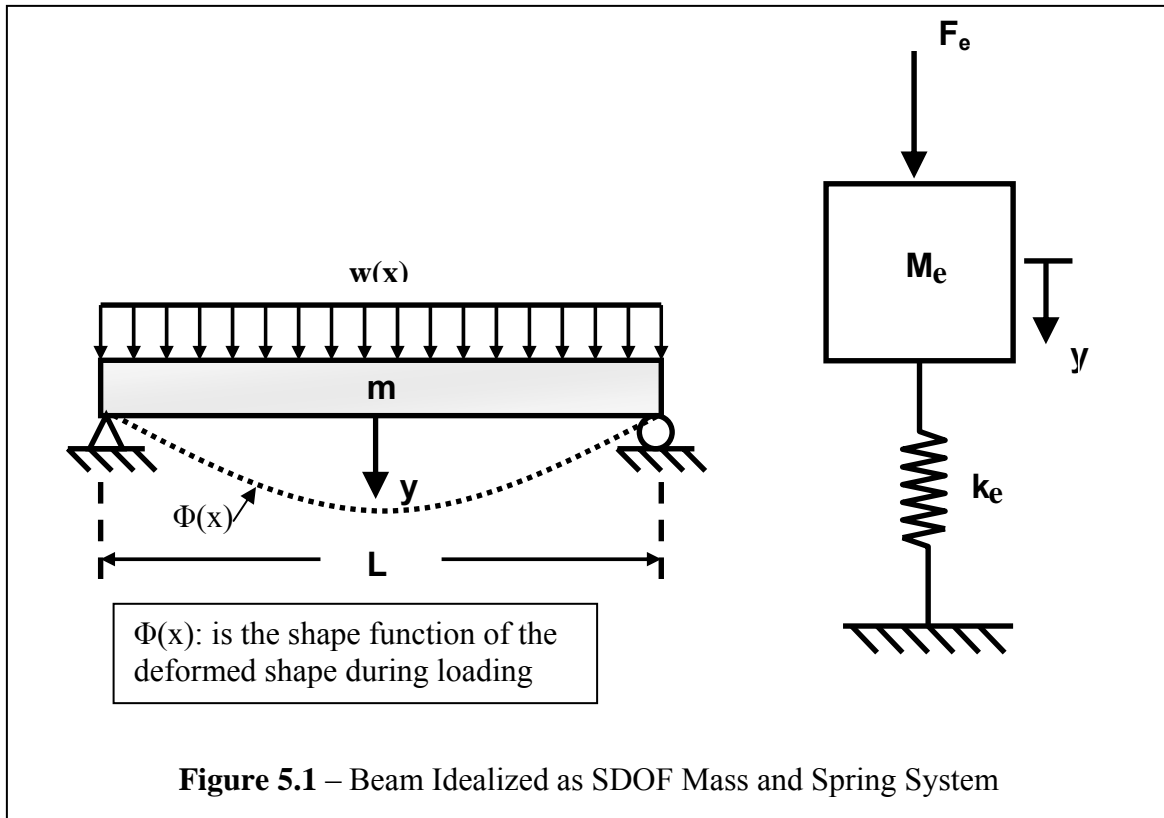
## 5.1 General

The dynamic modeling portion of this thesis will show how the polymer sheet on a CMU wall will behave under blast loading. It will predict whether or not the system will survive a blast load. There are two primary methods used for dynamic modeling: rigorous methods and numerical analysis. Numerical analysis, that is, solution of the differential equations of motion by arithmetic procedures, is much more general attack on the problem than rigorous methods, because the latter requires the loading and resistance functions be expressed by relatively simple mathematical terms (Biggs, 1964). Under blast loading, this is very difficult to accomplish. Throughout this chapter, a numerical analysis will be used with several approximations to ease the complexity of the design without eliminating the integrity of the design.

Most structures designed today can be idealized with a combination of springs and masses. For example a simply supported beam with a distributed loading can be idealized as an equivalent single degree of freedom (SDOF) spring a mass system shown in Figure 5.1. It is only necessary to formulate proper system parameters, such as effective load  $F_e$ , effective mass  $M_e$ , and effective stiffness  $k_e$ . Many of these constants are simply found such as  $M_e$  which is the mass of the total system and  $k_e$  which can be found from material properties of the beam since it is merely a ratio of force to deflection (Biggs, 1964).

For most dynamic modeling, the effects of damping is taken into account. However the effect may not be significant if the load duration is short and only the

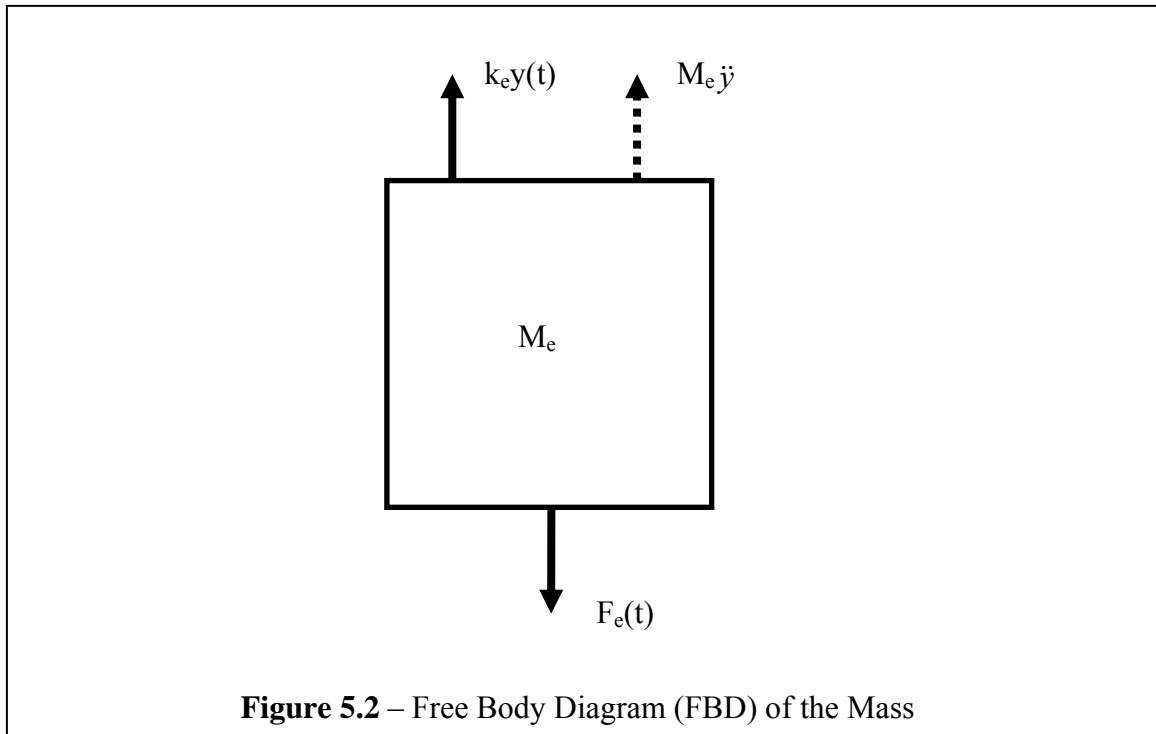
maximum dynamic response is of interest (Biggs, 1964). Since blast loads are defined by high pressures imparted over a very short duration, the effects of damping can be ignored for the dynamic modeling of a structural system under blast loading (Kiger and Salim, 1998).



## 5.2 SDOF Dynamic Modeling

Single degree of freedom system is defined to be a system in which only one type of motion is possible and can be defined in terms of a single coordinate. As for this case the mass in Figure 5.1 can only move in the vertical direction. This is how the polymer sheet will be designed for blast loading.

The first step in dynamic modeling is to isolate the mass and draw a free body diagram (Figure 5.2). To do this, external forces and the spring force  $k_e y(t)$  are applied. Additionally, the inertia force is applied to the mass, which is equal to the mass times the acceleration (Biggs, 1964).



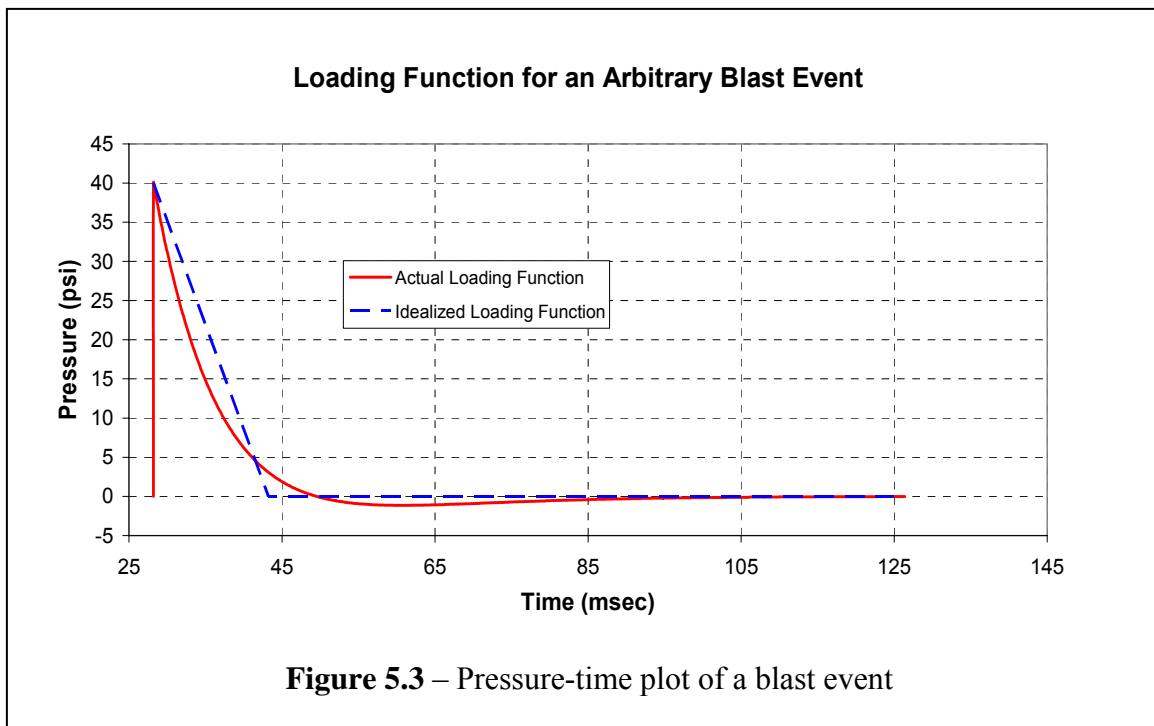
From equilibrium of FBD of Figure 5.2, the equation of motion becomes

$$F_e(t) - M_e \ddot{y}(t) - k_e y(t) = 0 \quad (5.1)$$

Where  $k_e y(t)$  is the static resistance function which was analytically modeled in Chapter 3.

In order to define an equivalent one degree system, it is necessary to evaluate the parameters of that system, namely,  $M_e$ ,  $k_e$ , and  $F_e$ . These parameters come from transformation factors which will be discussed later. Additionally, the load-time function

$F_e(t)$  must be established. A typical blast load is shown in Figure 5.3 which shows how the loading function is idealized. Typically, the negative phase of the loading function is conservatively ignored. However, it has been found that this region of the loading function reduced the deflection of the wall significantly and should be included. The idealized negative loading region is shown in Figure 5.4. Next, the equivalent system is selected so that the deflection of the concentrated mass is the same as that for some significant point of the structure, such as the mid-point. The constants of the equivalent system are then evaluated on the basis of an assumed shape of the actual structure. This shape will be taken to be the same as that resulting from the static application of the dynamic loading (Biggs, 1964).



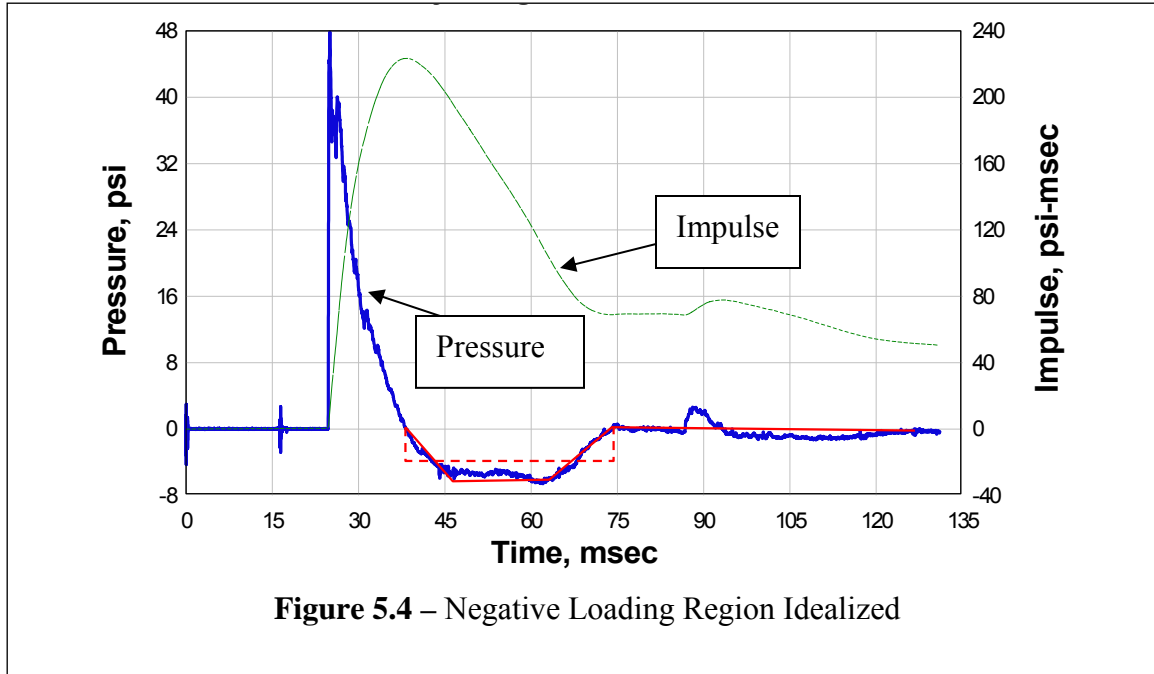


**Figure 5.4 – Negative Loading Region Idealized**

For convenience, transformation factors  $K$ , are used to convert the real system into the equivalent system. When the total load, mass, resistance, and stiffness of the real structure are multiplied by the corresponding transformation factors, the equivalent one-degree system factors are obtained (Biggs, 1964).

Each of the transformation factors comes from Biggs book *Introduction to structural dynamics(1964)*. The equivalent mass  $M_e$ , of the equivalent one-degree system for a structure with continuous mass, is given by

$$M_e = \int^L m\Phi^2(x)dx \quad (5.2)$$

Where:

$m$  = mass per unit length

$\Phi$  = is the assumed-shape function on which the equivalent system is based

Now the mass factor  $K_m$ , is introduced, which is defined as the ratio of equivalent mass to the actual total mass of the structure.



$$K_M = \frac{M_e}{M_T} \quad (5.3)$$

For the purpose of this thesis the above parameters are:

$$\begin{aligned} M_t &= mL \\ L &= \text{span of the beam} \\ M &= \text{given by equation (5.2)} \end{aligned}$$

By substituting these parameters into Equation (5.3),  $K_m$  can be written as:

$$K_M = \frac{1}{L} \int_0^L \phi^2(x) dx \quad (5.4)$$

The equivalent force on the idealize system for a beam with continuously distributed force along the entire length of the beam is given by the equation:

$$F_e = \int_0^L w(x)\phi(x) dx \quad (5.5)$$

Where:

$$\begin{aligned} w(x) &= \text{applied distributed load} \\ \phi(x) &= \text{assumed shape function} \end{aligned}$$

The load factor  $K_L$  is defined as the ratio of equivalent to actual total force.

$$K_L = \frac{F_e}{F_T} \quad (5.6)$$

For the beam shown in Figure 5.1,  $F_t = wL$  and  $F_e$  is given by Equation (5.5).

The resistance of an element is the internal force tending to restore the element to its unloaded static position. Thus the maximum resistance is the total load having the given distribution which the element could support statically. The stiffness is numerically equal to the total load of the same distribution which would cause a unit deflection at the point where the deflection is equal to that of the equivalent system. Due to this the resistance factor  $K_R$  is equal to the load factor  $K_L$  (Biggs, 1964).

$$K_R = \frac{R_{me}}{R_m} = K_L \quad \text{and} \quad K_R = \frac{k_e}{k} = K_L \quad (5.7)$$

Where:

$K_L$  = given by equation (5.6)

$R_m$  = is the maximum value of  $wL$ , or the plastic-limit load which the beam could support statically

$R_{me}$  = same as  $R_m$  but for the equivalent system

$k$  = is the value of  $wL$  which would cause a unit elastic deflection at mid span

Resistance and deflection are related in the elastic range by  $R = ky$  for the real structure and  $R_e = k_e y$  for the equivalent system.

The load mass factor  $K_{LM}$ , which is merely the ratio of the mass and load factors can now be used in the equation of motion, which is convenient since the equation can be written in terms of that factor alone. Equation (5.1) can now be written in the form of the real system with equivalent transformation factors:

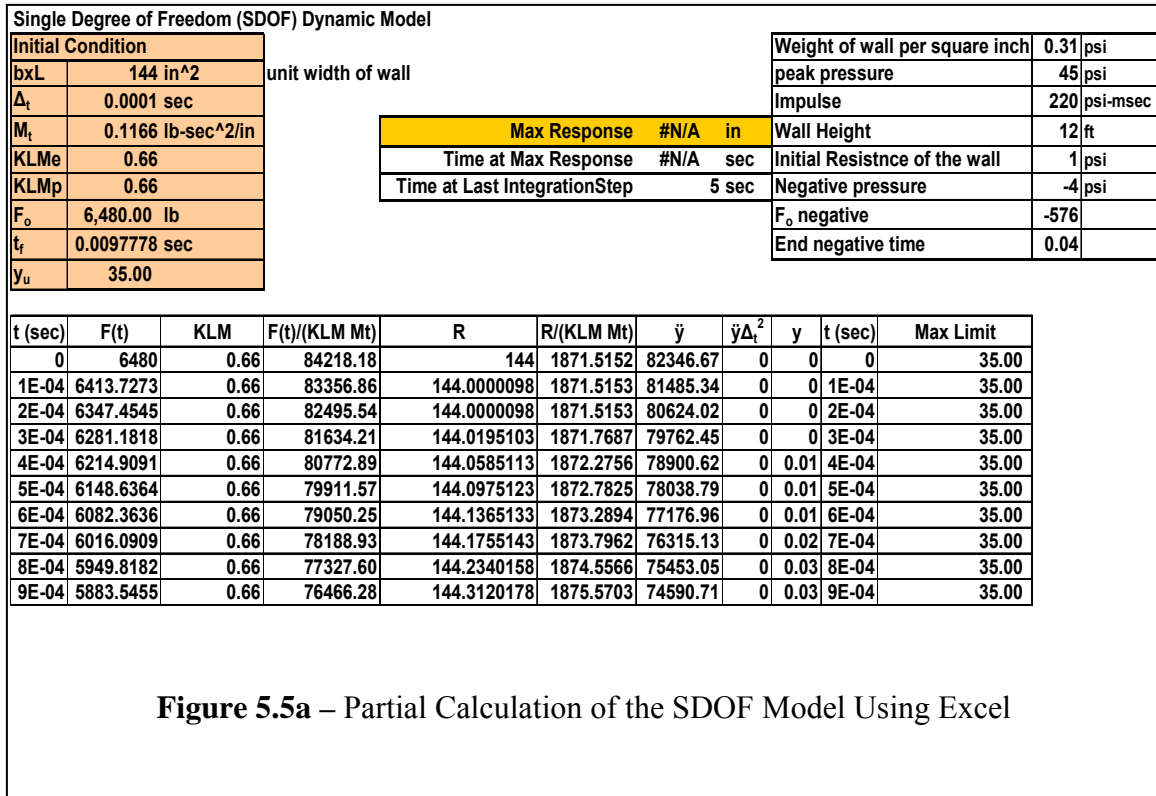
$$K_{LM} M_T \ddot{y}(t) + ky(t) = F(t) \quad (5.8)$$

Replacing  $ky(t)$  with the static resistance function  $R(t)$ , the equation becomes:

$$K_{LM} M_T \ddot{y}(t) + R(t) = F(t) \quad (5.9)$$

### 5.3 Application of Dynamic Modeling

Numerical analysis described in Biggs (1964) can now be used to solve for  $y(t)$  term. In order to find deflection for each incremental time interval, an excel sheet was designed (Figure 5.5a).



The steps for using the excel sheet is outlined in Biggs book and are as follows. The first step is to input parameters into the tables shown in Figure 5.5 i.e. area of wall, incremental time step, mass of the wall, K<sub>LM</sub> factor, peak pressure, impulse of the blast, etc. Once the factors are in the first incremental time is set which is 0. The next parameter is F(t) which is calculated at time 0 from a known blast. The parameter R comes from the analytical model predicted in Chapter 3. The acceleration and the deflection is calculated using equations from Biggs 1964.

$$y^{(s+1)} = 2y^s - y^{(s-1)} + \ddot{y}^s (\Delta t)^2 \quad (5.9)$$

Where

- y<sup>(s+1)</sup> = Incremental deflection after y<sup>s</sup>
- y<sup>s</sup> = Present deflection
- y<sup>(s-1)</sup> = Incremental step before y<sup>s</sup>
- ÿ = Acceleration
- Δt = Incremental time step

From this equation, it can be seen to calculate a deflection the previous deflection must be known. The first deflection will be set at 0 and then the second deflection cannot be found using equation (5.9) because only  $y^s$  is known and  $y^{(s-1)}$  is not. In order to calculate this deflection the following equation is used.

$$y^1 = \frac{1}{2} \ddot{y}^0 (\Delta t)^2 \quad (5.10)$$

Now  $y^{(s-1)}$  is equal to 0 and  $y^s$  is equal to  $y^1$ . After the first calculation, equation (5.9) is used for the remainder of the calculations. Additionally, to calculate  $\ddot{y}$  the following equation can be used.

$$\ddot{y} = F(t)/(K_{LM} M_t) - R(t)/(K_{LM} M_t) \quad (5.11)$$

Where

- F(t) = Force as a function of time
- $K_{LM}$  = Equivalent SDOF factor discussed above
- R(t) = Resistances as a function of time
- $M_t$  = Total mass of the Wall

The calculation is then performed until the maximum deflection is reached.

This prediction gives the deflection versus time of the polymer sheets. The procedure was also implemented into a user-friendly PC-Code, AFWAC (Air Force Wall Analysis Code). The opening screen of AFWAC is shown in Figure 5.5b.

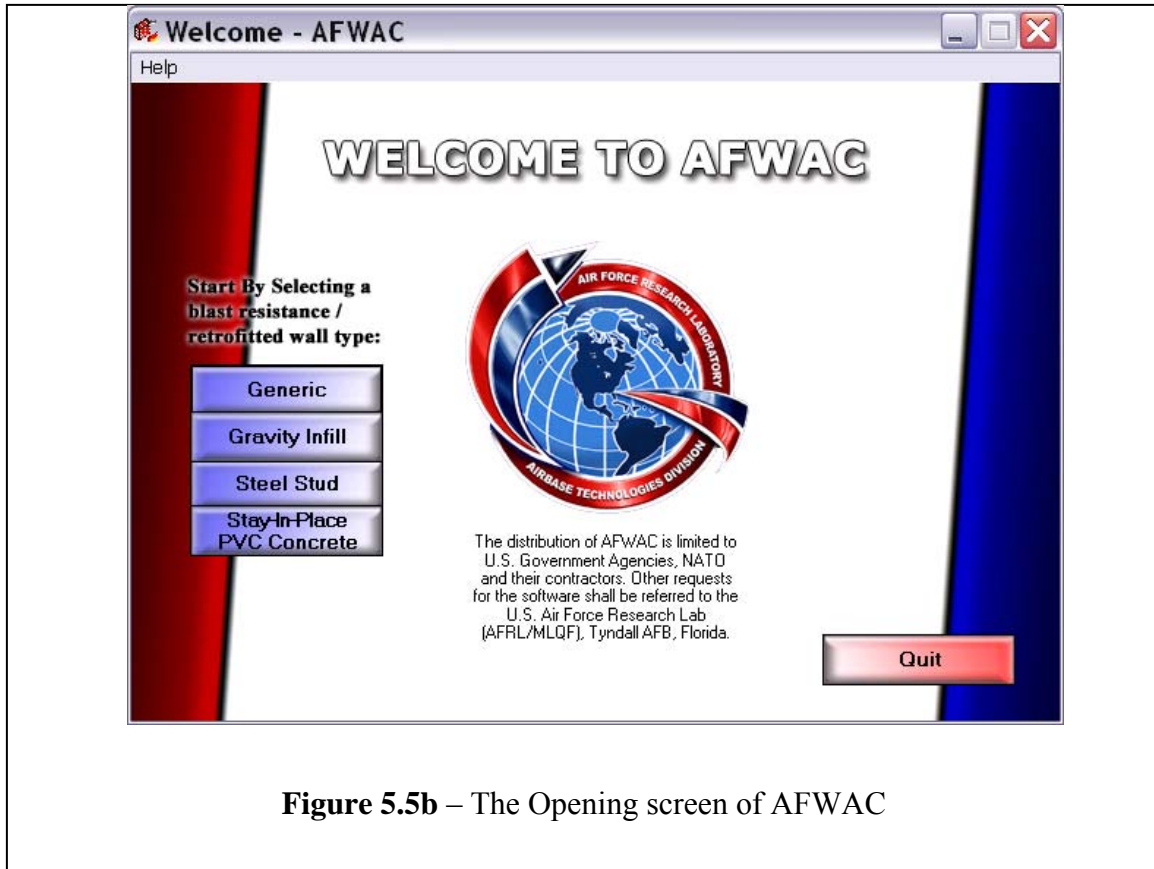
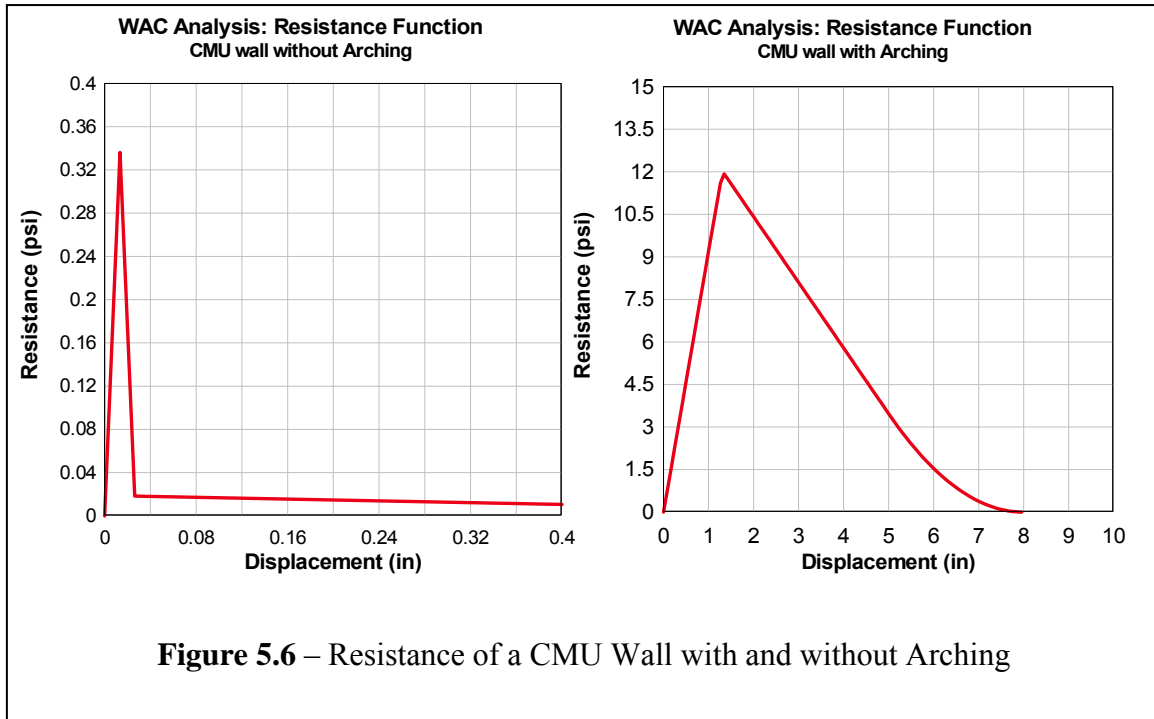


**Figure 5.5b** – The Opening screen of AFWAC

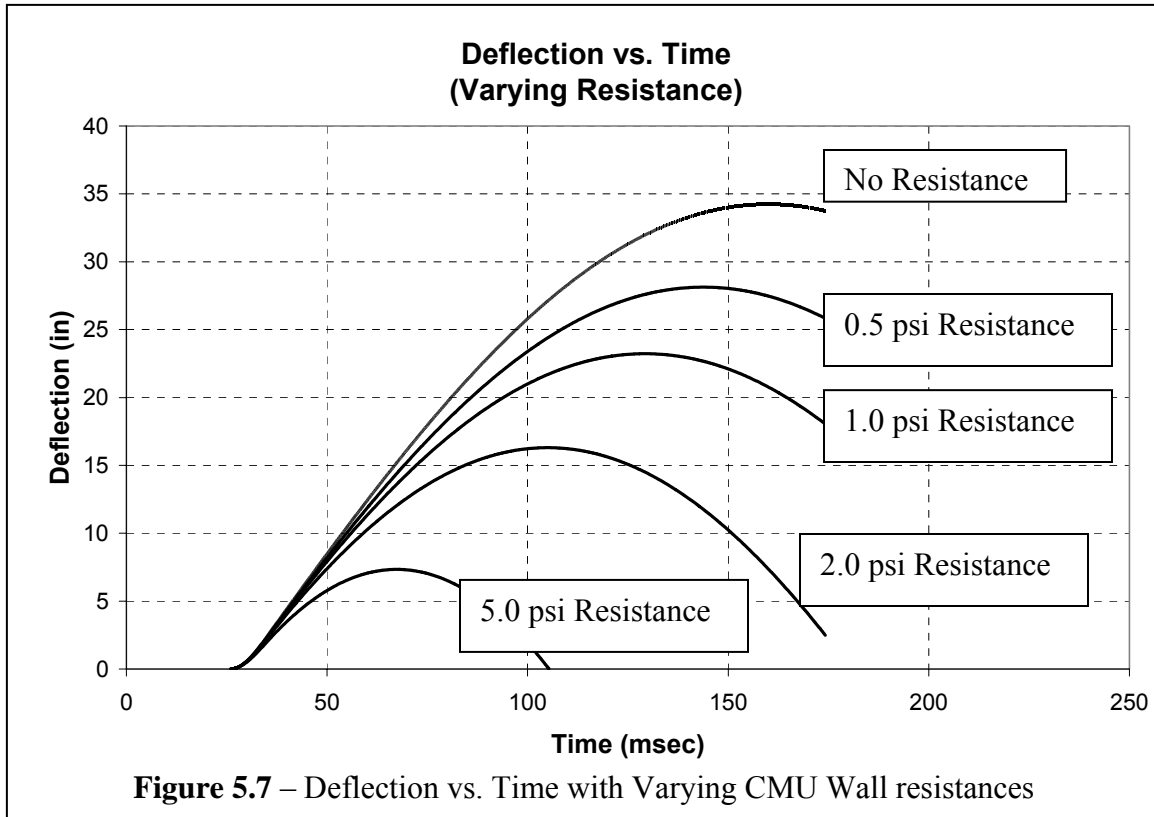
### **5.3.1 Effect of CMU wall resistance on the Dynamic Response**

However there is additional resistance provide by the CMU wall itself. This resistance depends on the amount of arching that occurs in the wall. The resistance, provided by arching, depends on the gap between the top of the CMU wall and the ceiling. When the shockwave hits the wall, the CMU wall cracks and pushes against the floor and ceiling. If there is a gap between the top of the CMU wall and the ceiling, the CMU wall does not arch until the gap is closes. Since the walls that are being retrofitted are non-load bearing infill CMU walls, there is typically a 1 inch gap between the CMU wall and the ceiling. This gap causes the delayed arching effect, which reduces the resistance of the wall. From a wall analysis code prepared by the United States Army

Corps of Engineers Research and Development Center called WAC, this procedure was done on a CMU wall without reinforcement. The findings are shown in Figure 5.6.



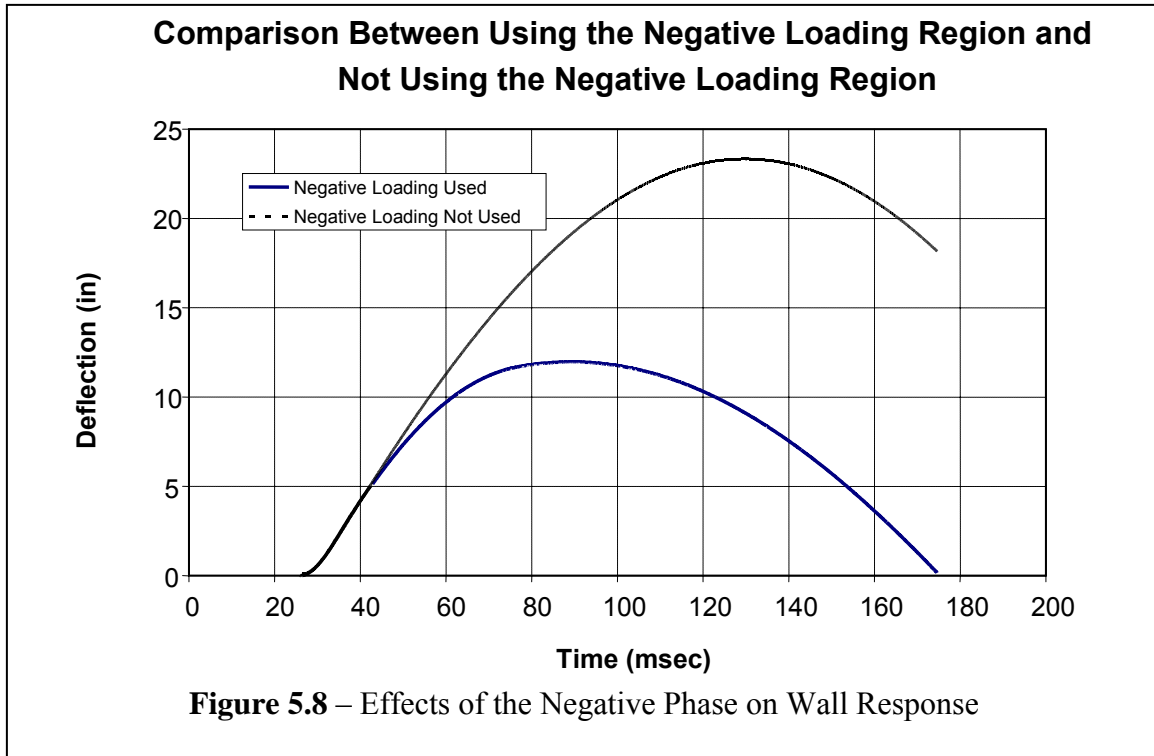
From Figure 5.6 it can be seen that the CMU wall provides 0.34 psi resistance without arching and 12 psi resistance with arching. Because of this a series of plots were made with varying the amount of resistance the CMU wall provided (Figure 5.7). From the plots it can be seen that picking a correct resistance of the CMU wall can make a large difference in the response of the wall. Based on experimental testing and knowledge from blast design experts a value of 1 psi will be used for the resistance of the CMU wall.



### 5.3.1 Effect of Negative Phase on the Dynamic Response

Once the resistance of the wall and the resistance of the polymer are found, the loading function must be analyzed. A typical blast loading has a positive and a negative region (Figure 5.7). Typically, the negative region is conservatively ignored. However, if the negative region is taken into account, it can provide significant resistance to the initial positive load. A graph was made comparing the effects of the negative loading region of a blast and is shown in Figure 5.8. From the graph it can be seen that by using the negative loading region the maximum deflection reduces by 11 inches.

The predicted resistance will now be compared to field testing done at the United States Air Force base to verify these results. The resistance function will be predicted using an assumed initial resistance of the CMU wall, and the negative phase of the loading will not be ignored.



## 5.4 Field Testing

Several walls have been tested using live explosions for various retrofit systems. As stated in Chapter 2, many retrofit systems such as steel studs, steel sheathing, and several different types of polymers have been tested under blast loading. In this section, the behavior of three polymers will be predicted using the procedure outlined in this thesis and compared to the experimental data received by the United States Air Force Research Laboratory. The first polymer will be the same polymer analyzed in Chapters 3 and 4. The second will be CUE polymer tested by the Air Force in a retrofitted system. The third is a polymer made by Bayer that was tested by the Air Force along with the CUE polymer. This second and third polymer is done to show that the procedure outlined in this thesis can be used for other types of polymers.

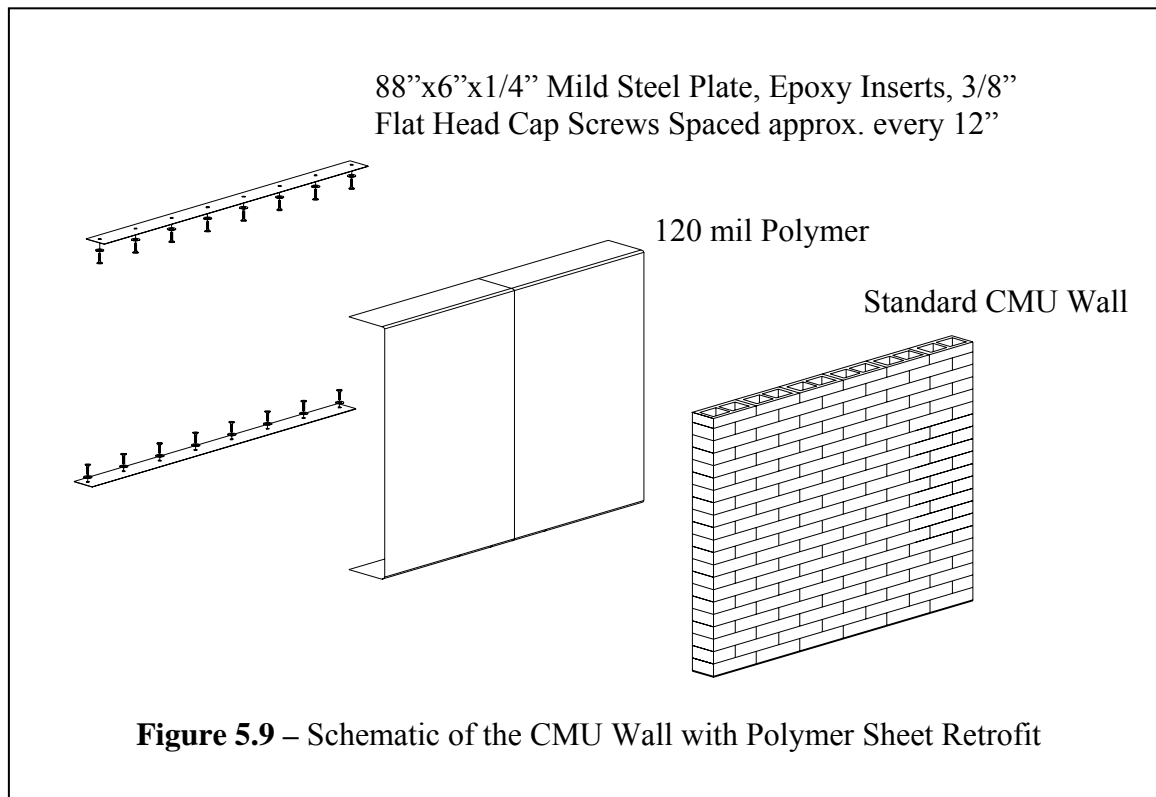


### **5.4.1 Polymer Sheets**

In this section the polymer sheets analysis in the previous Chapters will be compared with the results of the live testing data. Test setups, before and after photos, and predictions of the walls' behavior are made.

#### ***5.4.1.1 Test Setup***

Polymer sheets were anchored behind a typical CMU wall. A 6 x ¼ inch connection plate braced down with 3/8" flat head cap screws spaced approximately every 12" (Figure 5.9) was used. An undisclosed bomb was placed a certain distance away from the target to be used to load the retrofitted system. Pressure gages were placed around the wall along with deflection gages measuring the deflection at the middle of the wall.



Photos were taken before and after the wall had been loaded. Figure 5.10 shows the CMU wall with and without the polymer retrofit. From this figure, the connection plate used to connect the polymer to the floor and roof can be seen. Figure 5.10 also shows the device that measured midpoint deflection.



**Figure 5.10** – CMU Wall with and without Polymer Sheet Retrofit

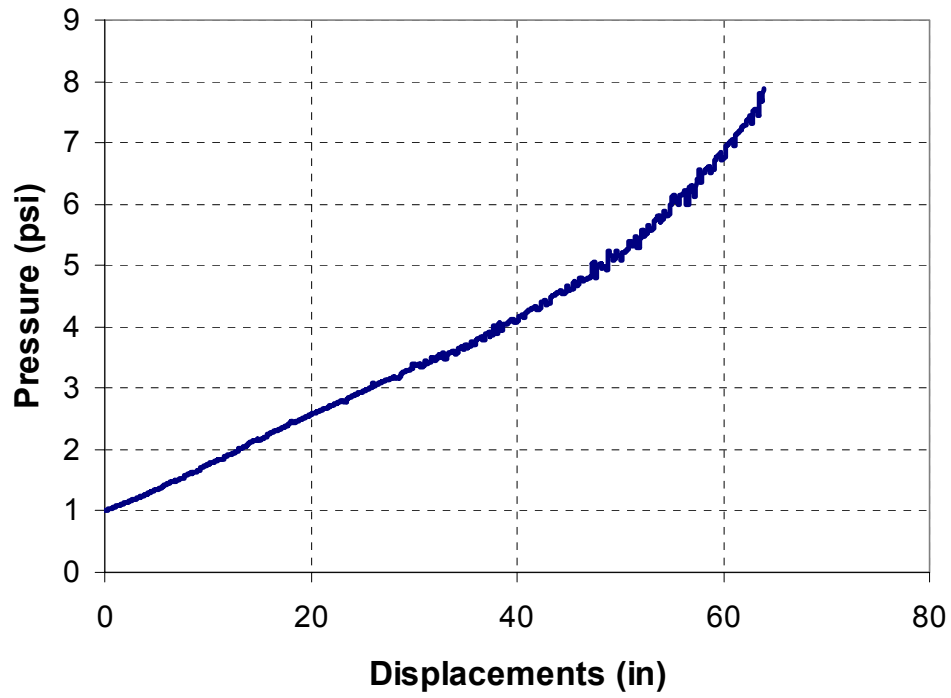
Figure 5.11 shows the outside and inside of the wall after explosion. From this figure it can be seen that the polymer retrofit is still intact. Although some of the CMU block did fall from the wall, none of the blocks entered the protected room. From these figures it can be seen that the retrofitted wall is capable of withstanding a blast load.



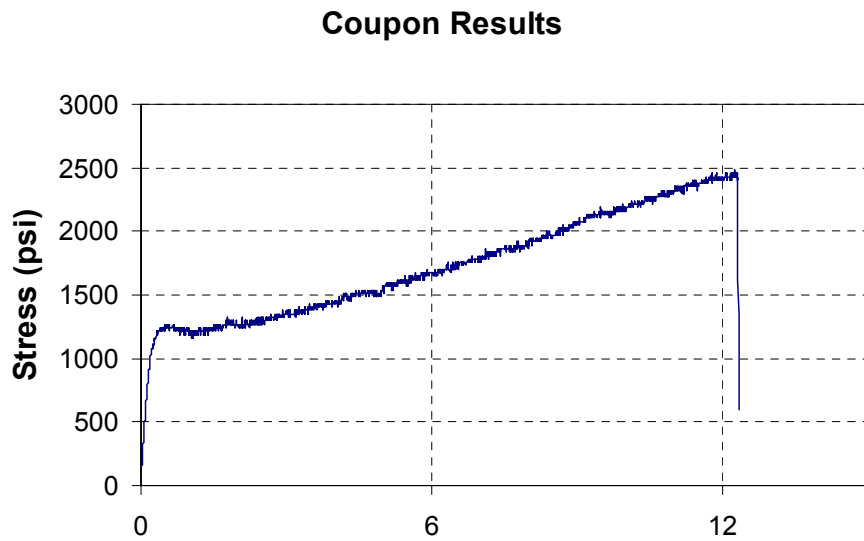
**Figure 5.11** – Outside and Inside of Wall after Explosion

#### **5.4.1.2 Results**

For this polymer the analytical model that was developed in this thesis was used in the SDOF which was used to compare to the results of the experimental results. The analytical model is shown in Figure 5.12a, which is developed using material response shown in Figure 5.12b for a representative coupon result.

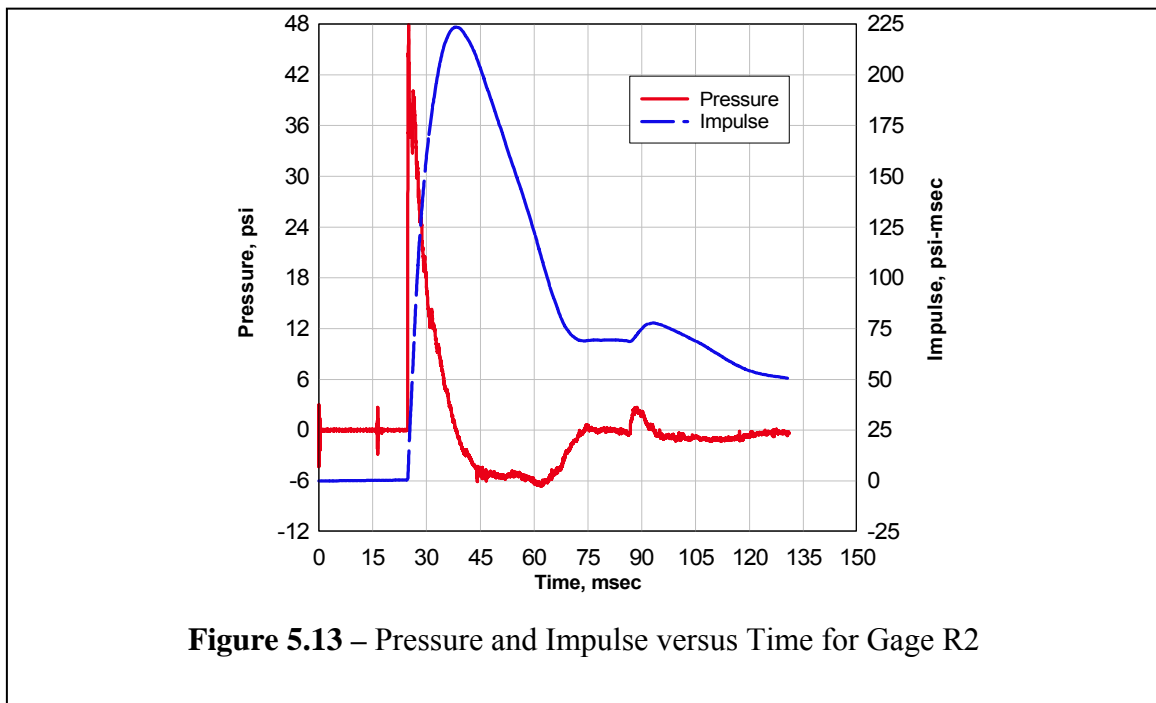


**Figure 5.12a** – Analytical Model of the Static Resistance Function



**Figure 5.12b** – Stress-Strain Relationship for the LifeShield Polymer

Three gages, R2, R3, and R4, were used to measure the pressure of the blast event. The pressures for each gage were recorded and an impulse was calculated and plotted versus time (Figure 5.13-5.15). The pressures and impulses were averaged and used for the input in the SDOF. Additionally, a deflection gage positioned at the mid-span of the CMU wall was used to make a graph of deflection versus time. Then this actual deflection versus time graph was compared to the predicted SDOF model of the wall. The results are shown in Figure 5.16. The results show an almost perfect match concluding that the SDOF predicted the response of the wall very well. There is approximately 12% error, but this could be attributed to the lack of information on the resistance of the CMU wall



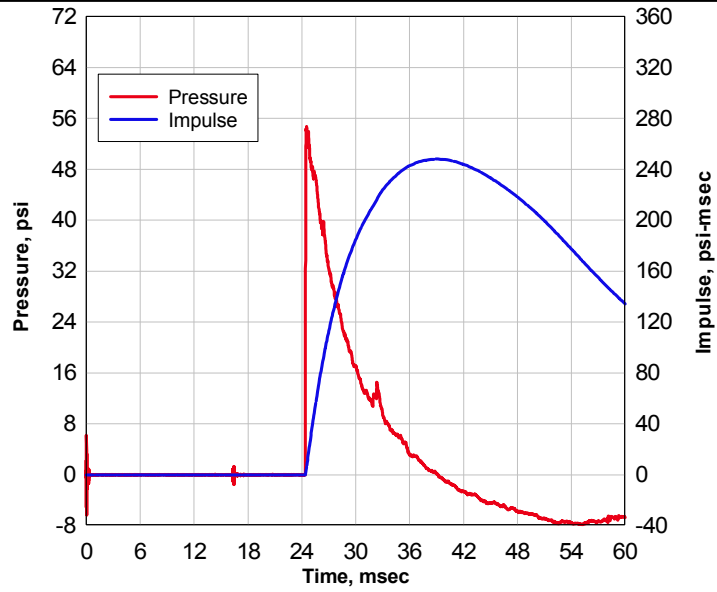


**Figure 5.14** – Pressure and Impulse versus Time for Gage R3

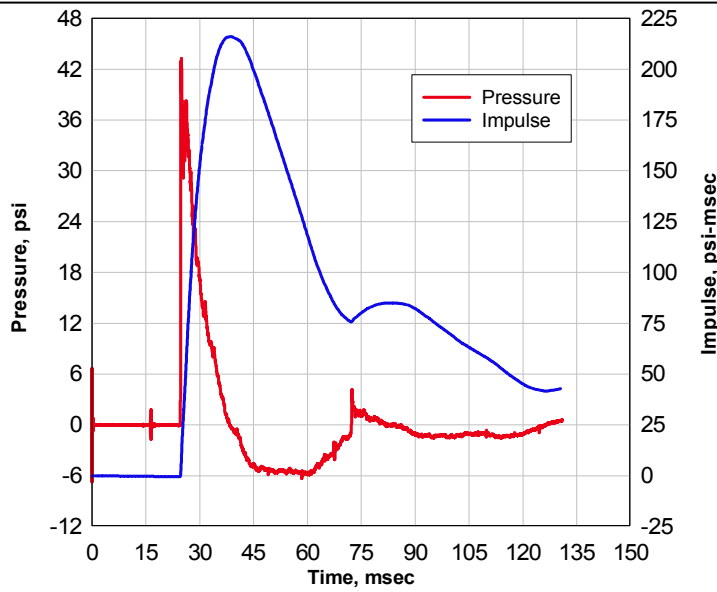


**Figure 5.15** – Pressure and Impulse versus Time for Gage R4

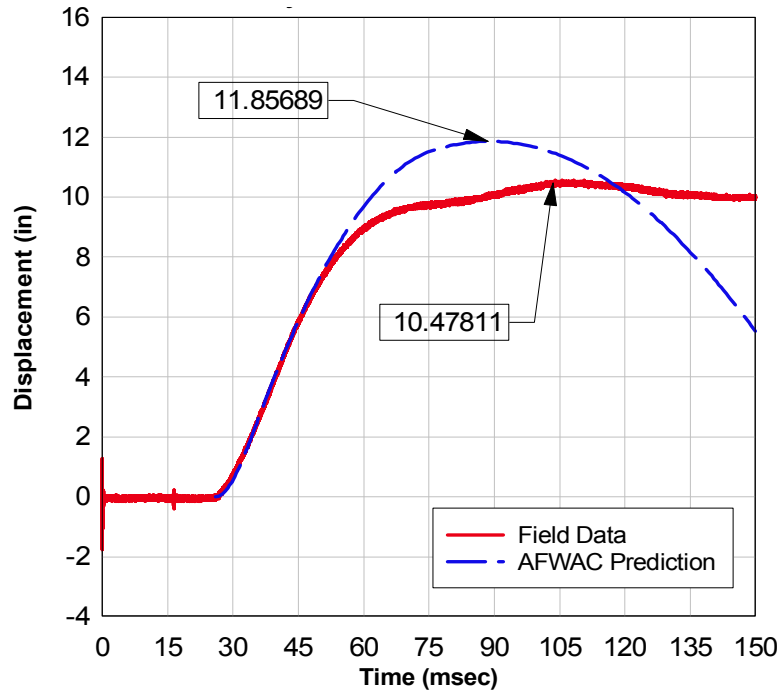


**Figure 5.16** – Comparison of the Predicted SDOF Model to the Actual response of LifeShield polymer retrofit

### **5.4.2 CUE Polymer**

Red polymer was also tested by the United States Air Force. In this section an analytical model will be predicted as shown in Chapter 3 of this thesis. This will be used to develop a SDOF model as shown in Chapter 5 of this thesis. Then the results of this SDOF model will be compared to the finding from the live testing.

#### ***5.4.2.1 Test Setup***

The CUE polymer was anchored behind a typical CMU wall. A 6 x ¼ inch connection plate braced down with 3/8” flat head cap screws spaced approximately every 12” was used. An undisclosed bomb was placed a certain distance away from the target to be used to load the retrofitted system. Pressure gages were placed around the wall along

with deflection gages measuring the deflection at the middle of the wall. For the comparison, the middle pressure gage will be used.

Before the test, photos were taken of the test setup. Figure 5.17 shows the CUE polymer on the inside of a CMU wall. Also shown is the device used to measure the deflection of the wall. Figure 5.18 shows how the CUE polymer was connected to the floor and ceiling.

Additionally, photos were taken after the test was conducted. Figure 5.19 shows the outside of the CMU wall after the test. The wall on the left is the one with the CUE polymer retrofit.



**Figure 5.17 – CMU Wall with CUE Polymer Retrofit**





**Figure 5.18** – CUE Polymer Connection



**Figure 5.19** – Outside of CMU Wall after Explosion

#### **5.4.2.2 Prediction**

The same procedure was used to develop an SDOF to compare with the experimental results. First, coupon tests were conducted to find the relationship between stress and strain. Figure 5.20 shows the coupon being stretched. Figure 5.21 shows a typical the relationship between stress and strain from the coupon testing. Once this is known, an analytical model (Static Resistance Function) was developed to be used by the SDOF. The analytical model is shown in Figure 5.22. Once the SDOF model was developed, a comparison was made between the experimental and the predicted results.

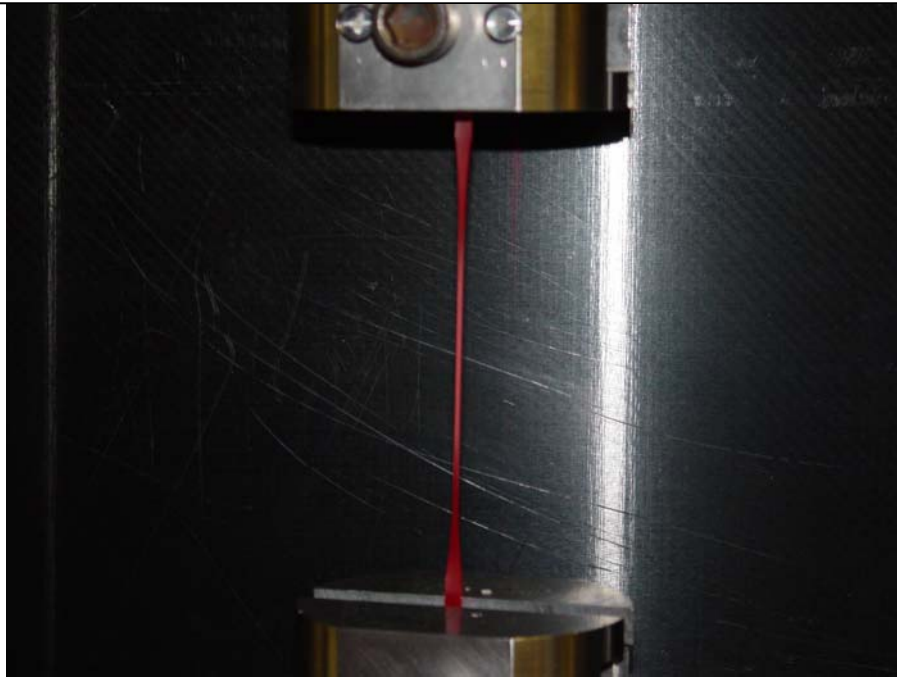


**Figure 5.20** – Coupon Testing of a CUE Sample

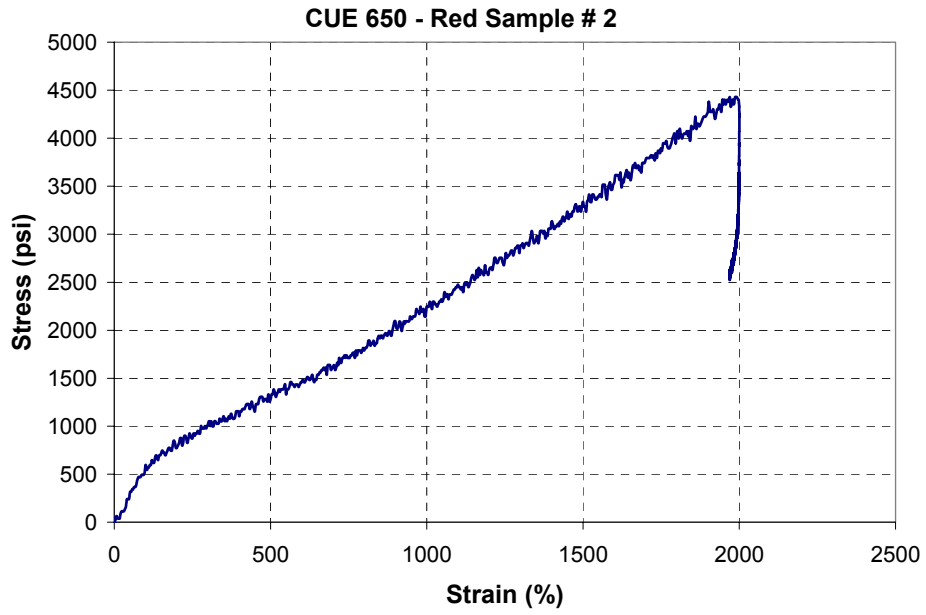


**Figure 5.21** – Coupon Results of a Typical CUE Sample

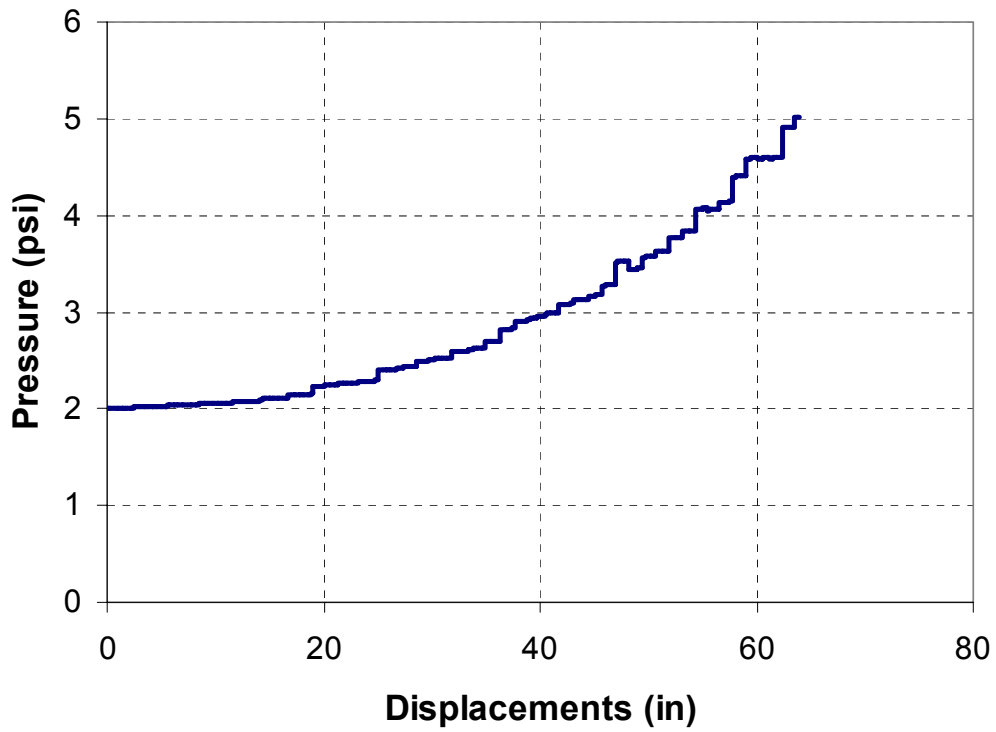


**Figure 5.22** – Analytical Model of CUE Polymer Sheets

### 5.4.2.3 Results

The pressure gage just to the right of the wall was used as the loading function for the SDOF (Figure 5.23). The SDOF and the experimental results were compared using a CMU wall resistance of 2 psi. It should be noted that the resistance provide by the CMU wall itself varies greatly with the amount of arching that occurs. It is recommended that further testing should be conducted on this topic. Finally the prediction and the actual results were compared and are shown in Figure 5.24. From the graph, it can be seen that the predicted model lines up quite well with the actual experimental results. There is approximately 18% error, but this could be attributed to the lack of information on the resistance of the CMU wall.

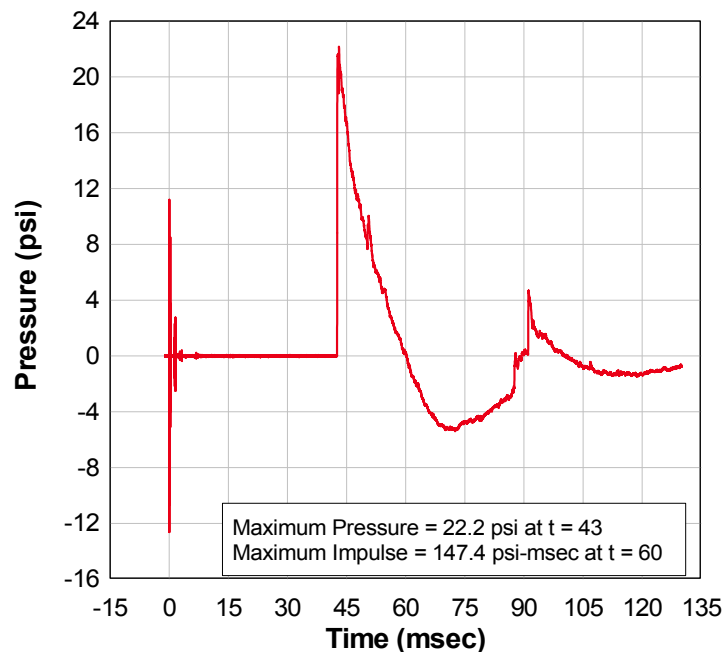


**Figure 5.23** – Loading Function from the Pressure Gage for the CUE Wall

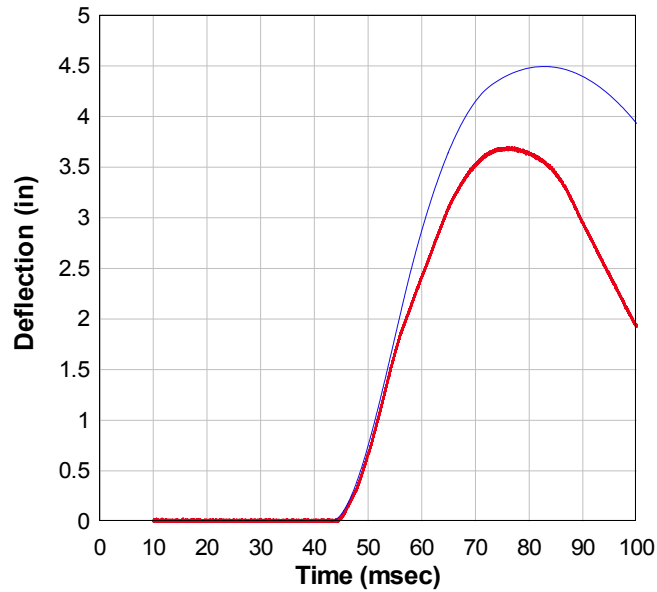


**Figure 5.24** – Comparison of the Predicted SDOF Model to the Actual response

### **5.4.3 Bayer Polymer**

Bayer polymer was also tested by the United States Air Force Research Lab. In this section, an analytical model will be predicted as shown in Chapter 3 of this thesis. This will be used to develop a SDOF model as shown in Chapter 5 of this thesis. Then the results of this SDOF model will be compared to the response of the wall measured during live testing.

#### ***5.4.2.1 Test Setup***

The Bayer polymer was sprayed on a typical CMU wall. The polymer was sprayed over the wall and extended along the floor and ceiling of the reaction structure. No mechanical connection was used to connect the polymer to ceiling and floor, instead the bond between the polymer and floors that was used to provide the necessary

anchorage. An undisclosed bomb was placed a certain distance away from the target to be used to load the retrofitted system. Pressure gages were placed around the wall, and a deflection gages measuring the deflection at the middle of the wall was used. For the comparison, the middle pressure gage will be used.

Before the test, photos were taken of the test setup. Figure 5.25 shows the Bayer polymer on the inside of a CMU wall. Also shown is the device used to measure the deflection of the wall. Additionally, photos were taken after the test was conducted. Figure 5.26 shows the outside of the CMU wall after the test. The wall on the right is the one with the Bayer polymer retrofit.



**Figure 5.25** – CMU Wall with Bayer Polymer Retrofit

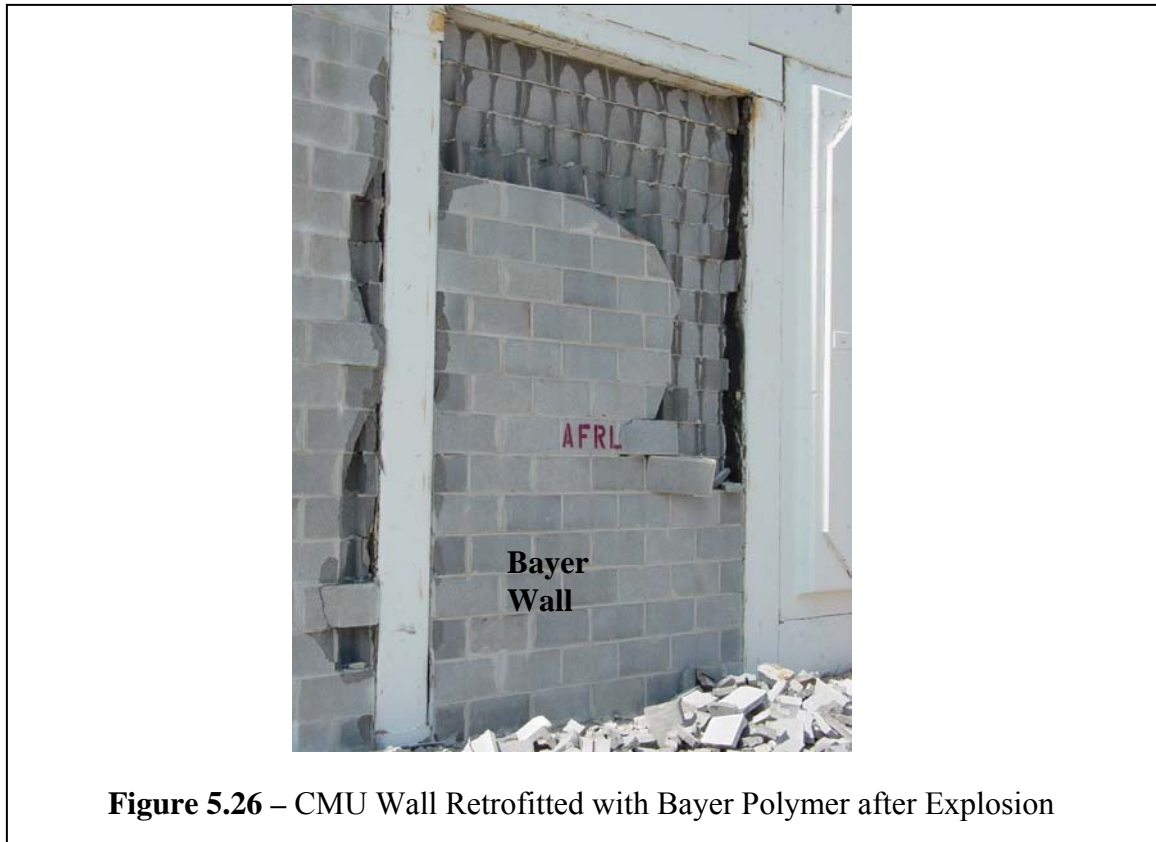


**Figure 5.26** – CMU Wall Retrofitted with Bayer Polymer after Explosion

#### ***5.4.3.2 Prediction***

The same procedure was used to develop an SDOF model to compare with the experimental results. First, coupon test were conducted to find the relationship between stress and strain. Figure 5.27 show the relationship between stress and strain for a typical coupon testing. Once this is known, an analytical model (Static Resistance Function) was developed to be used by the SDOF model. The analytical model is shown in Figure 5.28. Once the SDOF was developed, a comparison was made between the experimental and the predicted results.

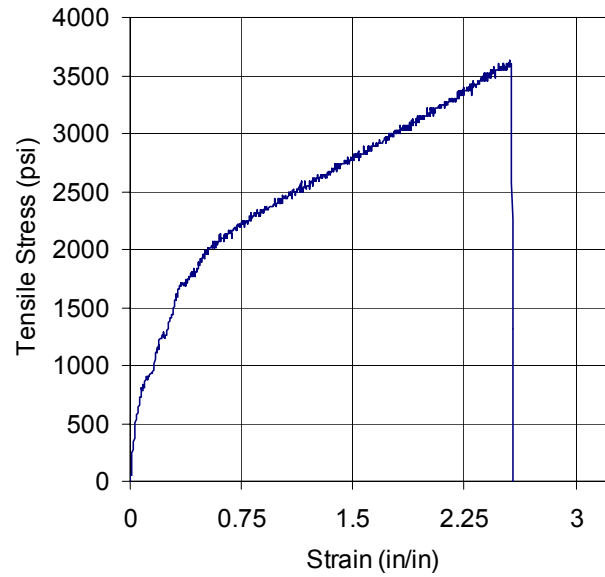


**Figure 5.27** – Typical Coupon Results of Bayer Polymer

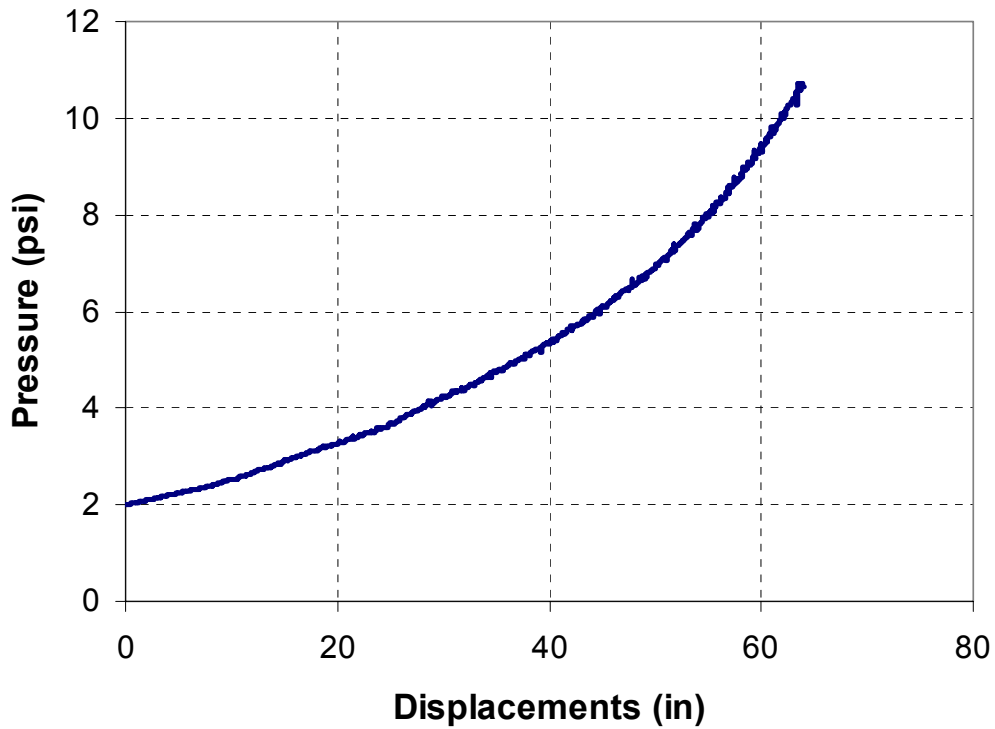


**Figure 5.28** – Analytical Model of Bayer Retrofit System



### 5.4.3.3 Results

The pressure gage just to the right of the wall was used as the loading function for the SDOF (Figure 5.29). The SDOF and the experimental results were compared using a CMU wall resistance of 2 psi. As stated above, this is arbitrary and should be researched more. Finally, the prediction and the actual results were compared and are shown in Figure 5.23. From the graph, it can be seen that predicted model lines up quite well with the measured response. There is approximately 18% error which can be attributed to the information the resistance of a CMU wall.

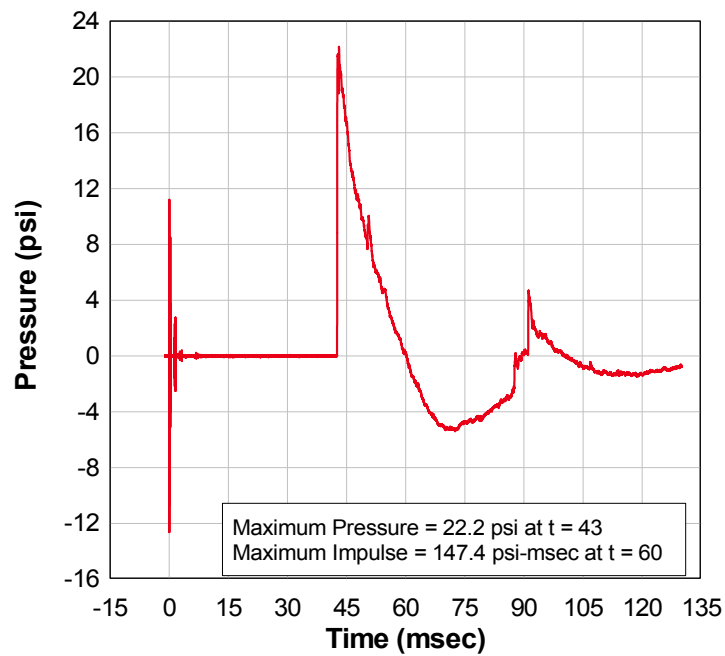


**Figure 5.29** – Loading Function from the Pressure Gage

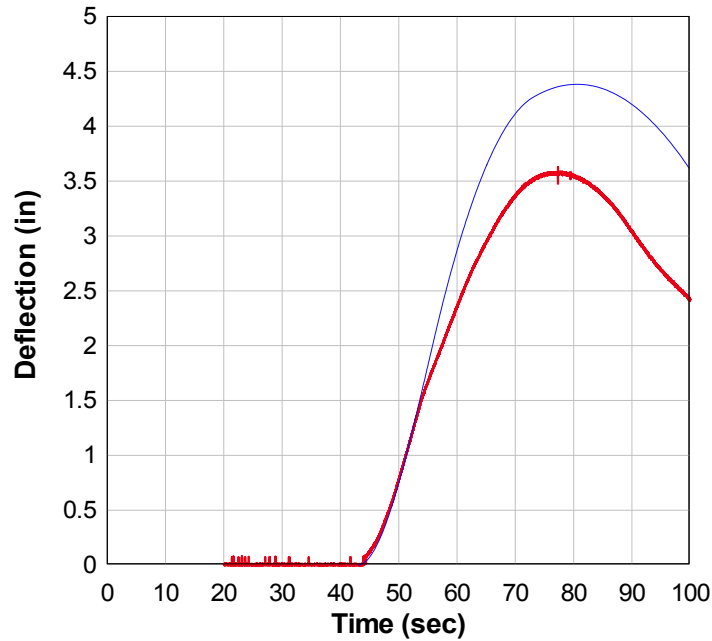


**Figure 5.30** – Comparison of the Predicted SDOF Model to the Actual response of Bayer Polymer retrofit system

## 5.5 Summary and Conclusions

SDOF Dynamic modeling is very useful in idealizing a complicated structure into an equivalent model with simple analysis. All of the predictions model the behavior of the retrofitted system very well based on some assumptions regarding the resistance of the CMU walls. The research developed in this thesis is implemented into the computer code AFWAC to be used to design blast retrofitted walls using polymers. Additionally, dynamic modeling has shown that these polymers are an efficient way to retrofit CMU walls. They limit the amount of debris that projects into a room and provide sufficient strength to ensure the room will not collapse on the occupants.

## CHAPTER 6 – CONCLUSIONS AND RECOMMENDATIONS

In this thesis, an analytical model verified by experimental data was used to develop engineering design methodology for blast-retrofit of CMU walls using polymer sheets. The results were then implemented in to the computer program AFWAC. This research has found that polymer sheets provide stability and ample ductility to CMU wall during a blast loading event.

- From the coupon tests, it was found that the polymer sheets have the ability to provide enormous amounts of energy absorption capabilities if allowed to develop to its full capacity.
- From the connection tests, it was found that to utilize the polymers full energy absorption capabilities a 6 x ¼ inch connection plate and bolt spacing of 12 or 16 inches can be used.
- As the thickness of the polymer increased, the accuracy of the analytical prediction decreased. Since there was only two thicknesses tested and four tests conducted, there should be further research conducted to explore more samples with variable thicknesses.
- Both the 16 inch and 12 inch spacing performed the same in the component testing section. 16 inch bolt spacing is recommended for the use in design practices of the polymer sheets used in this thesis.
- Both the 0.125 inch and 0.16 inch thickness of the polymer provide adequate ductility for the use in retrofit design.

- The polymer sheets showed under live testing that they provided adequate resistance to blast loading. Additionally, the polymer sheets limited the amount of debris that came into the room and provided adequate resistance to collapse of the walls. Polymer sheets proved to be a good material to retrofit CMU walls for blast design.
- It was found that the resistance of the CMU wall has a significant effect on the response of the polymer-CMU wall retrofit system. It is a recommendation of this thesis that more testing should be done to find a more accurate CMU wall resistance based on end conditions.
- The negative phase of the blast loading was found to significantly affect the predicted response of the wall system. Therefore, it is recommended that the negative phase not be ignored in the design of CMU wall retrofit with polymer sheets
- The failure of the CMU-polymer wall system could be controlled by ductility limits of the polymer and/or by tear strength due to localized stress concentrations areas at the edge of the clamping plate or at mortar joints. Therefore, it is recommended that additional research be conducted to develop predictive models of failure limit states that can be included into AFWAC.
- Little is known about the long-term effect of wear and erosion will have on the polymers. Especially, for the spray on polymer as the bond between the polymer and the CMU wall may decrease. More testing should be done on this subject.

## REFERENCES

- AFWAC (2005), Air Force Wall Analysis Code. Preliminary version developed by the University of Missouri-Columbia for the Air Force Research Laboratory, Version 1.1. December 2005.
- Albert, M. (2001). "Strengthening of Unreinforced Masonry Walls Using FRPs." *Journal of Composites for Construction*. American Society of Civil Engineers. Paper No. 21441. Reston, VA.
- Beckman, S. (2005). "Evaluation of Polymer Retrofit of CMU Walls for Blast Protection." Honors Thesis, University of Missouri-Columbia, Department of Civil and Environmental Engineering, Columbia, MO 65211-2200.
- Bechtold, J. (2004). "Evaluation of Polymer Retrofit Systems for Concrete Masonry Unit (CMU) Wall Systems Evaluation of the Concrete-Polymer Interaction." Honors Thesis, University of Missouri-Columbia, Department of Civil and Environmental Engineering, Columbia, MO 65211-2200.
- Biggs, J. M. (1964). *Introduction to Structural Dynamics*, McGraw-Hill, Inc., New York.
- Davidson, J. (2004). "Explosive Testing of Polymer Retrofit Masonry Walls" *Journal of Performance of Constructed Facilities*. American Society of Civil Engineers. Vol. 18, Number 2, pp 100-106. Reston, VA.
- Davidson, J. (2005). "Failure Mechanisms of Polymer-Reinforced Concrete Masonry Walls Subjected to Blast." *Journal of Structural Engineering*. American Society of Civil Engineers. Vol. 131, Number 8, pp 1194-1205. Reston, VA.
- Dinan, R. (2005). "Blast Resistant Steel Stud Wall Design." Doctoral Dissertation, University of Missouri, Department of Civil Engineering, Columbia, MO 65211-2200.
- Hilti (2001). *Systems and Solutions Customer Catalogue* [Brochure]. Tulsa, OK.
- Kennedy, J (2005). Analytical and Experimental Evaluation of Steel Sheets for Blast Retrofit Design. Masters Thesis, University of Missouri-Columbia, Department of Civil Engineering, Columbia, MO, 65211-2200
- Lane, J (2003). *Modeling and Design of Explosion Resistant Steel Stud Wall Systems*. Masters Thesis, University of Missouri, Department of Civil Engineering, Columbia, MO, 65211-2200.

Kiger, S. and Salim, H. (1998) “Use and Misuse of Structural Damping in Blast Response Calculations”, Concrete and Blast Effects, ACI Special Publication SP-175, pp.121-130.

Stone, H. and Engebretsen, J. “The Basics of Blast Resistant Design” Proc. 70<sup>th</sup> Annual Convention, Structural Engineers Association of California. pp. 87-94.